A brainstem to hypothalamic arcuate nucleus GABAergic circuit drives feeding

Pablo B Martinez de Morentin[†*1,2], J Antonio Gonzalez[1], Georgina K.C. Dowsett[3], Yuliia Martynova[1], Giles S.H. Yeo[3], Sergiy Sylantyev*[1], Lora K Heisler[1]

[1]The Rowett Institute, University of Aberdeen, UK.

[2]School of Biomedical Sciences, Faculty of Biological Sciences, University of Leeds, UK

[3]MRC Metabolic Diseases Unit, Wellcome-MRC Institute of Metabolic Science, Addenbrooke's Hospital, University of Cambridge, CB2 0QQ, United Kingdom.

[†]Lead author

*Correspondence

p.demorentin@leeds.ac.uk

s.sylantyev@abdn.ac.uk

ORCIDs:

PBM 0000-0002-0684-3215

JAG 0000-0001-7045-4831

GKCD 0000-0002-2134-8554

YM 0000-0003-1927-3298

GSHY 0000-0001-8823-3615

SS 0000-0002-1358-0601

LKH 0000-0002-7731-1419

Highlights

- Nucleus of the solitary tract (NTS) GABA neurons are responsive to nutritional status.
- Chemogenetic $GABA^{NTS}$ neuron activation reduces food intake and body weight.
- $GABA^{NTS}$ projections to the hypothalamic arcuate nucleus (ARC) promote satiety.
- Optogenetic $GABA^{NTS}$→ARC stimulation inhibits orexigenic AgRP/NPY neurons.

In Brief

Martinez de Morentin et al. identify GABAergic neurons in the nucleus of the solitary tract as a new player in the circuit governing feeding behavior and body weight.

Abstract

The obesity epidemic is principally driven by the consumption of more calories than the body requires. It is therefore essential that the mechanisms underpinning feeding behavior are defined. The brainstem nucleus of the solitary tract (NTS) receives direct information from the digestive system and projects to second order regions in the brain. Though γ-Aminobutyric acid is widely expressed in the NTS ($GABA^{NTS}$), its function has not been defined. Characterization of GABA cells using single nucleus RNA sequencing (Nuc-Seq) identified at least 19 clusters. Here we provide insight into the function of $GABA^{NTS}$ cells, revealing that selective activation of $GABA^{NTS}$ neurons significantly controls food intake and body weight. Optogenetic interrogation of $GABA^{NTS}$ circuitry identified $GABA^{NTS}$→arcuate nucleus of the hypothalamus (ARC) projections as appetite suppressive without creating aversion. Electrophysiological analysis revealed $GABA^{NTS}$→ARC stimulation inhibits hunger promoting agouti-related protein/neuropeptide Y (AgRP/NPY) neurons via GABA release. Adopting an intersectional genetics strategy, we clarify that the $GABA^{NTS}$→ARC circuit induces satiety. These data identify $GABA^{NTS}$ as a new modulator of feeding behavior, body weight and controller of orexigenic AgRP/NPY activity, thereby providing insight into the neural underpinnings of obesity.

Keywords

y-Aminobutyric acid, agouti-related -peptide, Neuropeptide Y, nucleus of the solitary tract, food intake.

Introduction

Obesity represents a key challenge to human health and is primarily due to the consumption of calories in excess to body's energy requirements. Eating is a complex behavior that not only depends on the basic energy demands at a cellular and organism level, but also the integration of internal and environmental cues, the reward value of food, motivation, and conditioning behavior (Andermann & Lowell, 2017; Campos et al., 2022). The aim of the present study was to probe neurocircuitry regulating feeding and body weight with the objective of uncovering critical energy homeostasis circuitry.

One of the primary nodes for the integration of energy-related information from the periphery to the brain is the nucleus of the solitary tract (NTS) within the brainstem dorsal vagal complex (DVC)(Hyun & Sohn, 2022). The NTS contains a heterogeneous population of energy-related sensitive cells(Cheng et al., 2022; Dowsett et al., 2021; Grill & Hayes, 2012). Recent studies using single-nucleus RNA sequencing provide a detailed expression map of identified cellular populations involved in energy balance, and most were revealed to be glutamatergic(Dowsett et al., 2021; Ludwig et al., 2021). For example, subpopulations of these glutamatergic cells influencing energy balance include leptin receptor (LEPR)(Cheng et al., 2020), calcitonin receptor (CALCR)(J. Chen et al., 2020a), glucagon-like peptide 1 receptor (GLP-1R)(Alhadeff et al., 2017; Fortin et al., 2020), preproglucagon (PPG)(Holt et al., 2019), tyrosine hydroxylase (TH) (Aklan et al., 2020; J. Chen et al., 2020b), cholecystokinin (CCK) (D'Agostino et al., 2016) and proopiomelanocortin (POMC) (Georgescu et al., 2020; Zhan et al., 2013). However, very little is known about the role of NTS inhibitory GABA-releasing clusters ($GABA^{NTS}$) in energy homeostasis. One report in rats indicated a subpopulation of GLP-1R-expressing neurons releasing GABA are necessary mediators for the anorectic effects of the obesity medication liraglutide (Fortin et al., 2020). Therefore, $GABA^{NTS}$ represents and intriguing and understudied population of NTS cells and is the focus of the present study.

In the regulation of feeding behavior, one of the most widely studied projections from the NTS is to the hypothalamus (Aklan et al., 2020; Blevins et al., 2004; D'Agostino et al., 2016; Liu et al., 2017; Shi et al., 2021; Tsang et al., 2020). However, whether the arcuate nucleus of the hypothalamus (ARC) receives GABAergic inhibitory control from the NTS is not known. Within the ARC is a subpopulation of potent orexigenic neurons expressing both agouti-related peptide and neuropeptide Y (AgRP/NPY) (Betley et al., 2013; Hahn et al., 1998;

89 Heisler et al., 2006; Heisler & Lam, 2017). We hypothesized that GABA^{NTS} neurons
90 significantly regulate feeding and body weight and project to and inhibit key hunger-
91 stimulating AgRP/NPY cells.

92

93 **Results**

94 *GABA^{NTS} cells are sensitive to energy status and modulate food intake*

95 To characterize GABA^{NTS} neurons, we initially used a single nucleus RNA sequencing
96 (NucSeq) dataset of the mouse dorsal vagal complex (Dowsett et al., 2021). Neuronal cells
97 expressing transcripts for *Slc32a1* (solute carrier family 32 member 1 or vesicular GABA
98 transporter, Vgat) were extracted and re-clustered, consisting of 1847 neurons, which formed
99 19 clusters (**Figure 1A**). Of these clusters, 2-Cacna2d1/Tmem163 expressed Vglut2
100 transcripts, and lower levels of *Gad1* and *Gad2.* Low expression of classical neurotransmitter
101 related genes was found in these GABAergic neuronal clusters (**Figure 1B**). Adipocyte
102 hormone Leptin receptor (*Lepr)* expression was identified in 13-Onecut2/Lepr and 15-
103 Ebf2/Acly clusters (**Figure 1B**). We identified some expression of incretin receptors including
104 glucagon-like receptor 1 (GLP-1R) and gastric inhibitory polypeptide receptor (GIPR) in
105 several clusters (**Figure S1A**). Differential gene expression analysis was performed on each
106 cluster to identify the effects of an overnight fast on transcript expression in GABAergic
107 (*Slc32a1*+) neurons (**Figure S1B**). Cluster 3-Dcc/Cdh8 displayed significant upregulation in
108 transcript expression in response to a fast, however 93.7% of this cluster originates from *ad*
109 *libitum* fed animals. Significantly differentially regulated genes in *Slc32a1*$^{+}$ neurons can be
110 found in **Figure S1C**. These data indicate minimal overlap with specific populations of NTS
111 neurons that have been previously described with regards to energy balance.

112 We therefore, examined whether GABA^{NTS} cells are responsive to energy status. We
113 facilitated the visualization of GABA^{NTS} neurons by crossing *Vgat-ires-Cre* mice with
114 *tdTomato$^{fl/fl}$* reporter mice (*Vgat^{tdTom},* **Figure 1D and 1E**). We then examined the expression
115 levels of the neuronal activity marker c-Fos (Olson et al., 1993) in mice that were overnight
116 fasted and in mice that were refed for 2 hours after overnight fasting. Re-fed mice showed
117 significantly more c-Fos in the NTS (**Figure S1D**) and specifically an increased number of
118 GABAergic cells activated (**Figure 1F and 1G**) when compared to fasted mice. This suggests
119 that GABA^{NTS} cells are responsive to positive energy status.

120 To determine whether $GABA^{NTS}$ neurons have a role in the control of food intake, we used
121 chemogenetic Designer Receptors Exclusively Activated by Designer Drugs (DREADD) to
122 manipulate $GABA^{NTS}$ cellular activity (Alexander et al., 2009). Specifically, AAVs expressing
123 hM3Dq, hM4Di or control mCherry were bilaterally injected into the NTS of *Vgat*^{Cre} mice
124 (**Figure 1H**). This allowed to modulate $GABA^{NTS}$ neuron activity with the administration of the
125 designer drug clozapine-N-oxide (CNO). Administration of CNO in hM3Dq-injected mice
126 induced strong c-Fos expression in the NTS (**Figure 1I**). We next assessed the effect of the
127 modulation of $GABA^{NTS}$ on food intake in mice under different scenarios. In ad libitum fed
128 mice, hM3Dq chemogenetic activation of $GABA^{NTS}$ cells significantly reduced overall food
129 intake during the active dark cycle when compared to control (mCherry) siblings (**Figure 1J**
130 **and S1E**). Similarly, hM3Dq $GABA^{NTS}$ cell activation reduced food intake in hunger-induced
131 fasted mice when compared to control mice (**Figure S1F and S1G**). Conversely, hM4Di
132 chemogenetic inhibition of $GABA^{NTS}$ cell in satiated mice during the light cycle significantly
133 increased food intake when compared to satiated littermate mCherry controls (**Figure 1K**).

134 Given the potent reduction of food intake produced by the activation of $GABA^{NTS}$ neurons,
135 we examined whether prolonged activation impacted body weight. Twice-daily administration
136 of CNO (**Figure 1L)** in hM3Dq-expressing mice induced a significant reduction in daily food
137 intake (**Figure 1M**) and a progressive reduction in body weight (**Figure 1N and 1O**). Although
138 feeding returned to baseline levels 72 hours after the final CNO administration, body weight
139 remained significantly lower in hM3Dq-expressing mice (**Figure 1N**). In contrast, prolonged
140 $GABA^{NTS}$ neuron inhibition using hM4Di did not induce greater food intake (**Figure S1H**) nor
141 changes in body weight (**Figure S1I**) when compared to their littermate mCherry controls.
142 These results indicate that the selective activation of $GABA^{NTS}$ neurons is sufficient to result
143 in a sustained reduction in energy intake and hence body weight.

144 Recently, it has been reported that the inhibition of neurons expressing the GABA-producing
145 enzyme, glutamate decarboxylase (GAD), in the NTS of rats partially blunted the anorectic
146 effect of the GLP1-R agonist liraglutide (Fortin et al., 2020). These data, suggest that
147 $GABA^{NTS}$ contributes to the therapeutic effects of GLP1-R agonists in rats. However, GLP-
148 1R expression in rats and mice differs, especially its receptor density (Cork et al., 2015;
149 Graham et al., 2020; Jensen et al., 2018). We therefore assessed the feeding response of
150 liraglutide in $GABA^{NTS}$-hM4Di/mCherry-expressing mice. Chemogenetic inhibition of
151 $GABA^{NTS}$ partially blunted the acute anorectic effects of liraglutide (**Figure S1J and S1K**).
152 This provides support that $GABA^{NTS}$ participates in the anorectic effects of liraglutide in mice.

153

154 *Optogenetic stimulation of GABA^{NTS} terminals inhibits AgRP/NPY^{ARC} cells*

155 To clarify the circuitry through which GABA^{NTS} neurons influence feeding and body weight,
156 we used Channelrhodopsin 2 (ChR2)-assisted circuit mapping (CRACM) (González et al.,
157 2016; Petreanu et al., 2007). Specifically, an AAV expressing ChR2-mCherry was injected
158 into the NTS of *Vgat^{Cre}* mice (**Figure 2A**) and projection patterns were analyzed. GABA^{NTS}
159 cells project to hypothalamic subregions including the ARC, paraventricular nucleus (PVH)
160 and dorsomedial nucleus (DMH) and various other extra-hypothalamic regions (**Figure S2A**).
161 Within the ARC, we observed a dense array of projections (**Figure 2B**). This identified the
162 ARC as a candidate second order region involved in the GABA^{NTS} control of food intake and
163 body weight.

164 Fasting induces activation of AgRP/NPY-expressing neurons (Hahn et al., 1998) and direct
165 AgRP/NPY neuron activation induces robust feeding (Aponte et al., 2011; Krashes et al.,
166 2011). Since GABA-releasing neurons are the main inhibitory network in the brain (Krnjević
167 & Schwartz, 1967), we hypothesized that GABA^{NTS} cells projecting to the ARC would target
168 AgRP/NPY neurons to decrease food intake. To interrogate this potential
169 GABA^{NTS}→AgRP/NPY^{ARC} circuit, *Vgat^{Cre}* were crossed with *Npy^{hrGFP}* mice (*Vgat^{Cre}::Npy^{hrGFP}*)
170 and bilaterally injected with AAV-ChR2-mCherry into the NTS. We observed that a subset of
171 NPY^{hrGFP} cell bodies were surrounded by mCherry-containing fibers (**Figure 2C**). In contrast,
172 terminals were not found surrounding neurons expressing other neuropeptides involved in
173 the regulation of food intake such as POMC neurons (Williams & Schwartz, 2005) (**Figure**
174 **2D**).

175 We next investigated whether this anatomical connectivity produced functional interactions
176 between GABA^{NTS} terminals and AgRP/NPY^{ARC} and POMC neurons. Specifically, photo-
177 stimulation of ChR2-containing axon terminals from GABA^{NTS} neurons produced robust
178 synaptic responses in 14% of AgRP/NPY cells in the ARC but not in POMC cells (**Figure**
179 **2E**). The rapid synaptic currents triggered in AgRP/NPY cells by the optical stimulation
180 changed polarity near the equilibrium potential for chloride (**Figure 2F and 2G**), as expected
181 from ionotropic GABA receptors. Light-induced currents were unexpectedly small, and their
182 reversal potential was more positive than that expected for GABA-activated currents (about
183 -60 mV) (**Figure 2H-J**). These effects could be explained by voltage- and space-clamp errors
184 (Spruston et al., 1993) and in turn suggest that perhaps GABA^{NTS} terminals reach ARC NPY

185 cells at dendrites distant from the soma. While it is not possible to directly demonstrate that
186 this is the case, we tested whether this reasoning was justified by simulating the optogenetic
187 activation of GABA synaptic events at distal vs proximal dendrites in a model neuron. Using
188 a predictive neuronal model (Lindroos & Hellgren Kotaleski, 2021), we found that GABAergic
189 post-synaptic currents become progressively smaller with their reversal potential
190 progressively more positive, the further the GABA inputs are from the soma (**Figure S2 B-**
191 **E**).

192 Next, we tested whether activation of GABA receptors at NPY cells is accompanied by
193 release of GABA from $GABA^{NTS}$ ChR2-containing terminals. We first stimulated ChR2-
194 mCherry expressing $GABA^{NTS}$ fibers in the ARC and performed a "sniffer patch" experiment
195 registering $GABA_AR$ single-channel openings above the NPY^{hrGFP} cells contacted by
196 $GABA^{NTS}$ fibers (**Figure 2K**). In this experiment, the $GABA_AR$ response was isolated with a
197 specific cocktail of antagonists (see Methods). This provides semi-quantitative monitoring of
198 extracellular levels of GABA (Sylantyev et al., 2020). A burst of light directed to $GABA^{NTS}$
199 ChR2-containing terminals in the ARC induced single-channel openings in membrane patch
200 in control conditions, and the currents had amplitudes comparable to GABAergic inhibitory
201 currents (Sylantyev et al., 2020) (**Figure 2L, *left***). Application of $GABA_AR$ competitive
202 antagonist gabazine reversibly blocked the single-channel openings (**Figure 2L, *middle and***
203 ***right*)**. The same pattern of receptor opening time was observed in all assessed patches
204 (**Figure 2M**). This suggested that postsynaptic NPY cells are sensitive to $GABA^{NTS}$
205 presynaptic release of GABA.

206 To test whether NPY cells were inhibited by the release of GABA from $GABA^{NTS}$ terminals,
207 we designed a protocol of additive subthreshold electrical stimuli. This method is designed to
208 evoke an action potential after 5 stimuli. In addition, we coupled a 470 nm light burst to the
209 same trigger (**Figure S2F**). We then alternated a sequence of electrical stimuli and electrical
210 stimuli with light burst. The electrical stimulation evoked an action potential(s) (**Figure S2G,**
211 ***left*)** followed by low-frequency or no single-channel openings in the sniffer patch. When we
212 coupled the electrical stimulation with the light burst, the occurrence of actions potentials was
213 blocked and accompanied with single-channel openings in a sniffer patch (**Figure S2G,**
214 ***right***). This happened in all cells patched (**Figure S2H**). These openings resembled $GABA_AR$
215 openings illustrated in Figure 2L. Subsequent stimulations showed a decrease in channel
216 opening intensity, suggesting a depletion of GABA stores from the presynaptic terminal,
217 which was eventually insufficient to prevent the action potential (**Figure S2I**). These results

218 provide strong evidence that $GABA^{NTS}$ fibers inhibit AgRP/NPY cells due to the release of the
219 fast neurotransmitter GABA.

220

221 *$GABA^{NTS}$→ARC optogenetic stimulation reduces feeding and is not aversive*

222 Given the dense fiber projection pattern of NTS-GABAergic cells to the ARC, and that its
223 activation induced a strong inhibition of AgRP/NPY neurons, we interrogated whether this
224 circuit is sufficient to influence food intake. To investigate this, AAVs expressing ChR2-
225 mCherry were infused into the NTS of *$Vgat^{Cre}$* mice and an optic fiber was placed above the
226 ARC (**Figure 3A**). Food intake was measured both without and with ARC photo-stimulation
227 prior to the onset of the dark cycle (**Figure 3B and 3C**). Light stimulation of $GABA^{NTS}$→ARC
228 terminals induced a strong acute inhibition of food intake that lasted 60 min from food
229 presentation, as compared to the same mice without light stimulation (**Figure 3D and 3E**).

230 The DVC has been proposed to be a key region modulating food intake reduction associated
231 with aversive states (D'Agostino & Luckman, 2022). To assess whether $GABA^{NTS}$→ARC
232 activation produces aversion or negative valence (Berridge, 2004; Betley et al., 2015), we
233 evaluated the existence of passive avoidance behavior using an adapted real-time place
234 preference (RTPP) task (D'Agostino et al., 2016; Kim et al., 2013; Stamatakis & Stuber,
235 2012). Specifically, in a two-sided open arena, light stimulus was coupled to one of the sides
236 (**Figure 3F**). $GABA^{NTS}$→ARC stimulation or lack of stimulation did not produce a place
237 preference (**Figure 3G**) and mice travelled a similar distance in both sides of the arena
238 (**Figure 3H**). These findings indicate that $GABA^{NTS}$→ARC stimulation does not produce
239 negative valence or aversion.

240 In addition to influencing homeostatic feeding, modulation of AgRP/NPY cells has also been
241 reported to elicit anxiety-like behaviors influencing exploration and foraging which impacts
242 food consumption (Dietrich et al., 2015; Heinz et al., 2021; Li et al., 2019). To test whether
243 the activation of the $GABA^{NTS}$→ARC circuit produced anxiety-related behavior, mice were
244 assessed in an open-field arena (OFA) and an elevated zero-maze task (EZM) (**Figure S2A**
245 **and S2D**). $GABA^{NTS}$→ARC stimulation did not alter the time mice spent in the center of the
246 OFA (**Figure S2B**). Likewise, mice displayed similar ambulatory patterns and travelled
247 comparable distance during the OFA test with and without $GABA^{NTS}$→ARC stimulation
248 (**Figure S2C**). Consistent with the OFA data, $GABA^{NTS}$→ARC stimulation did not alter either
249 the time (**Figure S2E**) or distance travelled in the exposed zones of the EZM (**Figure S2F**).

250 These results provide evidence that stimulation of the GABA^{NTS}→ARC circuit impacts feeding
251 without altering other behavioral states such as anxiety-like behavior.

252 We postulated that since our model involved fast neurotransmission rather than long term
253 release of neuropeptides, the reduction in food intake that we observed could begin by
254 reducing the interaction with the nutritional cue at first instance. To investigate this, we
255 designed a task where mice would first be allowed to explore an empty arena and then three
256 items would be presented at the same time, an inedible object, a novel palatable food item
257 and a known nutritional food item (**Figure 3I**). The number of interactions with each item was
258 measured with and without GABA^{NTS}→ARC stimulation. GABA^{NTS}→ARC stimulation did not
259 induce changes in the interaction with the novel object (**Figure 3J**), further suggesting that
260 GABA^{NTS}→ARC does not induce anxiety-like behavior. The number of interactions with the
261 novel palatable food item was increased under both non-stimulation and stimulation trials
262 (**Figure S2F and S2G**). However, we found that under optical stimulation mice had less
263 interactions with the known nutritional item (**Figure 3J and S2G**), suggesting that
264 GABA^{NTS}→ARC activation reduces hunger. Taken together, these findings indicate that
265 GABA^{NTS}→ARC stimulation decreases feeding and hunger without inducing aversion or
266 anxiety.

267

268 *GABA^{NTS}→ARC neuron activation promotes satiety*

269 We next used a two-virus intersectional approach (Fenno et al., 2014, 2017) to provide a
270 more detailed characterization of GABA^{NTS}→ARC activation in energy homeostasis. *Vgat^{Cre}*
271 mice were bilaterally injected with AAVs expressing Flipase recombinase (FlpO) (AAV-DIO-
272 FlpO) under the control of Cre into the NTS of *Vgat^{Cre}* mice, allowing us to express a second
273 recombinase only in GABA^{NTS} cells. After surgery recovery, a retrograde AAV encoding for a
274 FlpO dependent hM3Dq-mCherry (rgAAV-fDIO-hM3Dq-mCherry) was bilaterally injected into
275 the ARC to retrogradely deliver hM3Dq in a FlpO-dependent manner to GABA^{NTS} cells.
276 Therefore, hM3Dq was expressed only in GABA^{NTS} cells projecting to the ARC in *Vgat^{Cre}*
277 mice (**Figure 4A**).

278 Corroborating the optogenetic data presented above, the selective chemogenetic stimulation
279 of the GABA^{NTS}→ARC circuit significantly reduced acute food intake (**Figure 4B** and **4C**) in
280 ad libitum fed mice. GABA^{NTS}→ARC circuit activation did not alter overall locomotor activity

281 (**Figure 4D** and **4E**), respiratory quotient (**Figure 4F** and **4G**) or heat production (**Figure 4H**
282 and **4I**). GABA^{NTS}→ARC neuron activation also reduced food intake in refed mice after
283 overnight fasting (**Figure 4J**). Fasting is associated with a rise in systemic levels of ghrelin
284 (Cummings et al., 2001) which acts as a pre-prandial effector stimulating AgRP/NPY neurons
285 to initiate a feeding response (H. Y. Chen et al., 2004; Luquet et al., 2007). To examine
286 whether GABA^{NTS}→ARC neuron activation is sufficient to dampen a hunger cue,
287 GABA^{NTS}:hM3Dq-expressing mice were pre-treated with CNO prior to ghrelin. Activation of
288 the GABA^{NTS}→ARC neurons with CNO prevented the feeding induced by an orexigenic dose
289 of ghrelin (**Figure 4L and 4M)**. We next performed an analysis of the microstructure of the
290 feeding event during the anorectic episode produced by CNO (Clifton, 2000; Richard et al.,
291 2011; Zorrilla et al., 2005). GABA^{NTS}→ARC neuron activation reduced meal size (**Figure 4N**)
292 and significantly reduced the number of meal events in the earliest interval compared to saline
293 treatment (**Figure 4O** and **4P**). Taken together, these findings indicate that GABA^{NTS}→ARC
294 neuron activation is sufficient to blunt fasting and ghrelin-induced hunger and significantly
295 reduces food intake by promoting satiety.

296

297 **Discussion**

298 Here we identify a critical new brain circuit modulating appetite and body weight. We focused
299 on the NTS because it is a brain region positioned to receive and integrate energy-related
300 information from the periphery and relay it within the CNS to promote energy homeostasis.
301 However, the NTS is neurochemically heterogeneous and key neurons within it performing
302 this function have not been fully defined. Using multi-methodological approach, here we
303 identify GABA^{NTS} neurons as sufficient to control feeding behavior and body weight in mice.

304 Recent efforts to decode the function of specific chemically defined neurons within the NTS
305 have revealed that distinct subpopulations of glutamatergic cells play a role in energy
306 homeostasis (Dowsett et al., 2021). However, NTS inhibitory GABA-releasing neurons have
307 not been studied in detail and this is necessary to clarify the role of both excitatory and
308 inhibitory NTS signals in the regulation of energy balance (Cheng et al., 2022). Here we
309 provide a detailed characterization of the effect of GABA^{NTS} in the regulation of energy
310 homeostasis and body weight. A recent report provided evidence that obesity medication
311 liraglutide engages GABA^{NTS} neurons to reduce food intake in rats, providing a rationale that

312 activating $GABA^{NTS}$ cells may have translational relevance for the treatment of human obesity
313 (Fortin et al., 2020).

314 The NTS is involved in satiety and satiation, and refeeding induces a strong neuronal
315 activation in this region (D'Agostino et al., 2016; Wu et al., 2014). We discovered that
316 refeeding significantly activates a subset of $GABA^{NTS}$ cells. Further, we found that activation
317 of $GABA^{NTS}$ neurons with chemogenetics was anorectic, and controlled food intake and body
318 weight. Consistently, when we inhibited these neurons, we observed a potent induction of
319 feeding in satiated mice, suggesting a crucial role in the induction of early eating. However,
320 when the inhibition occurred in ad libitum mice entering the dark cycle, we didn't observe an
321 increased food intake. This could be explained by two reasons. First, despite of mice being
322 kept in ad libitum conditions, they are not satiated at the onset of the dark cycle, meaning
323 $GABA^{NTS}$ neuros are likely to not be active at this time, therefore an inhibition would not
324 meaningful. Second, during the active dark cycle there are multiple feeding cues not only
325 vagal sensory afferents but afferent from the sensory system that would modulate feeding
326 and could counteract $GABA^{NTS}$ lack of inhibition in second order neurons. Our data illustrates
327 that $GABA^{NTS}$ neurons project widely within the brain, with particularly dense innervation of
328 the hypothalamus. Several studies indicate that there is a coordination between the NTS and
329 the hypothalamus to orchestrate the meal event (Aklan et al., 2020; Blevins et al., 2004;
330 D'Agostino et al., 2018; Liu et al., 2017; Tsang et al., 2020). However, whether the ARC
331 receives inhibitory control from the NTS is not known and was examined here.

332 Given that GABA is an inhibitory neurotransmitter, we hypothesized that $GABA^{NTS}$ neurons
333 inhibit appetite stimulating neurons. We focused on $AgRP/NPY^{ARC}$ neurons because of the
334 dense $GABA^{NTS}$ innervation that we found and the potent orexigenic properties of AgRP/NPY
335 (Aponte et al., 2011; Krashes et al., 2011; Luquet et al., 2005). In addition, AgRP/NPY
336 neurons display a multiple timescale activation (Mandelblat-Cerf et al., 2015) that could
337 explain the lack of feeding effect during the chemogenetic inhibition of $GABA^{NTS}$. We
338 demonstrated that $GABA^{NTS}$ terminals in the ARC release GABA and that this is synchronized
339 with suppression of the action potential propagation postsynaptic $AgRP/NPY^{ARC}$ cells. The
340 timescale of $GABA_AR$ openings after optical stimulation in a membrane patch placed over the
341 $GABA^{NTS}$ terminal suggests the release of GABA from this terminal rather than from another
342 inhibitory neurons. The number of AgRP/NPY neurons responding is in line with the 20%
343 ARC responders to NTS innervation published previously (Aklan et al., 2020). However,
344 despite the relatively small number of $AgRP/NPY^{ARC}$ neurons inhibited by $GABA^{NTS}$ terminals,

345 it was sufficient to significantly reduce feeding in freely behaving mice. AgRP/NPY cells are
346 poised to orchestrate the integration of homeostatic, reward and sensory cues as well as
347 learning and conditioned behaviors (Aponte et al., 2011; Berrios et al., 2021; Deem et al.,
348 2022; Dietrich et al., 2012, 2015; Garau et al., 2020; Han et al., 2021; Jikomes et al., 2016;
349 Krashes et al., 2011, 2014; Wang et al., 2021). A detailed analysis of feeding behavior
350 revealed that activation of the $GABA^{NTS}$→ARC pathway specifically reduces hunger and
351 promotes satiety and does not induce negative valence, aversion or anxiety.

352

353 Obesity is an international health concern that is primarily the consequence of over-eating.
354 Defining the mechanisms governing hunger and food intake is therefore of paramount
355 importance. Here we identify a new player that controls appetite and body weight, $GABA^{NTS}$.
356 Specifically, we show that NTS GABA-releasing neurons are active during satiety and reduce
357 food intake and body weight without causing aversion or anxiety. We demonstrate that
358 $GABA^{NTS}$ cells directly activate $GABA_A$Rs on the surface of AgRP/NPY cells which inhibits
359 neuron activity. These studies reveal for the first time the effect of $GABA^{NTS}$ neurons on
360 feeding and body weight, and identify a fast inhibitory circuit between the NTS and the ARC
361 in the control of food intake. These results thereby provide significant insight into the brain
362 circuits governing appetite and body weight, findings of relevance to the global obesity crisis.

363 **Methods**

364 **RNA-Seq**

365 Single nucleus RNA-sequencing data from the mouse hindbrain in the fed and fasted state
366 was taken from (Dowsett et al., 2021). Neuronal nuclei expressing at least 1 UMI count for
367 *Slc32a1* were identified as GABAergic neurons, subsetted and reclustered using Seurat
368 package version 4.3 (Hao et al., 2021). Marker genes for each cluster were calculated using
369 Wilcoxon's rank-sum test. Each cluster was named with 2 marker genes that were expressed
370 in >60% of the cluster, <30% of the rest of the data and had an average log fold change >0.5.
371 If no genes fit these criteria, then the two genes with the lowest p-values were used.
372 Differential gene expression analysis between ad libitum fed and overnight fasted cells was
373 performed using the Wilcoxon's rank sum test. Feature plots were drawn using the Seurat
374 package and ggplot2.

375 **Animals**

376 *Vgat-ires-Cre* (Vong et al., 2011) (Slc32a1tm2(cre)Lowl; #016962), *NPY-hrGFP* (van den Pol
377 et al., 2009)(van den Pol et al., 2009)(van den Pol et al., 2009)(van den Pol et al., 2009)
378 (B6.FVB-Tg(Npy-hrGFP)1Lowl/J; #006417), POMC-dsRed (Hentges et al., 2009) (Tg(Pomc-
379 DsRed)18Low) and *Rosa26tdTomato-LoxP* (Madisen et al., 2009) (B6.Cg-
380 Gt(ROSA)26Sortm9(CAG-tdTomato)Hze/J, #007909) mice were obtained from The Jackson
381 Laboratory (Bar Harbor, USA) and bred in a C57Bl/6J background. Mice were fed with
382 standard laboratory chow (Standard CRM (P) 801722, Special diets, UK) and provided with
383 water ad libitum, unless otherwise stated. Mice were kept in a 12-hours light:dark cycle (7am-
384 7pm) in environmental controlled conditions (20-22°C and 40-60% RH). All experimental
385 procedures were performed in accordance with the UK Animal (Scientific Procedures) Act
386 1986.

387

388 **Viral vectors**

389 Cre-dependent viral vectors were purchased from Addgene, AAV8-hSyn-DIO-hM3D(Gq)-
390 mCherry ($1.83x10^{12}$ gc/ml) was a gift from Bryan Roth (Addgene plasmid # 44361) (Krashes
391 et al., 2011), AAVrg-hSyn-fDIO-hM3D(Gq)-mCherry-WPREpA ($1.8x10^{12}$ gc/ml) was a gift
392 from Ulrik Gether (Addgene plasmid # 154868); AAV8-hSyn-DIO-mCherry ($3.6x10^{12}$ gc/ml)
393 was a gift from Bryan Roth (Addgene plasmid # 50459); AAV8-pEF1a-DIO-FLPo-WPRE-

394 hGHpA (2x10^{12} gc/ml) was a gift from Li Zhang (Addgene plasmid # 87306) (Zingg et al.,
395 2017). AAV2-EF1a-DIO-ChR2(E123T/T159C)-mCherry and AAV2-EF1a-DIO-
396 ChR2(E123T/T159C)-YFP (7.3x10^{12} vp/ml) were a gift from Karl Deisseroth and were
397 obtained from University of North Carolina Vector Core (Chapel Hil, NC, USA). All viral
398 particles were delivered into nuclei-specific regions through stereotaxic injections.

399

400 **Stereotaxic surgeries**

401 For viral delivering in the NTS, stereotaxic surgery was adapted from previous studies
402 (D'Agostino et al., 2016). Briefly, 12-20 weeks old mice were anaesthetized with isoflurane,
403 back region of the neck shaved and placed in a stereotaxic instrument (David Kopf
404 instruments, CA, USA) with a face mask (World Precision Instruments, FL, USA). Head was
405 inclined ~70 degrees forward and a longitudinal incision was made in the skin at the level of
406 the C1; neck muscles were retracted to expose the atlanto-occipital membrane. This was
407 carefully dissected allowing access to the dorsal brainstem and visualization of the obex.
408 Using a pulled glass capillary (40µ tip diameter) (G1, Narishige, UK) and a pneumatic
409 microinjector (IM-11-2, Narishige, UK) 200-300 nl of viral preparation was bilaterally injected
410 into the NTS (obex: AP:0.25 mm AP, L:± 0.25 mm and DV:-0.25mm) at a flow of 50nl/min.
411 Capillary was left in the injection place for 5 min to allow diffusion and it was removed slowly
412 to avoid dispersion to neighbor brainstem regions. Viral delivery into the ARC was performed
413 as previously described (Wagner et al., 2022) at coordinates bregma: AP:1.58 mm AP,
414 L:±0.2mm and DV:5.90 mm. For optical fiber cannula placement, mice were allowed 4 weeks
415 recovery form the NTS surgery and a 200 µm core diameter, 0.39NA (CFMLC, Thorlabs, UK)
416 optical fiber implants were placed in the third ventricle above the ARC. Mice were allowed 3
417 weeks before any study to allow surgery recovery and maximal viral expression. Post hoc
418 analysis of injection site, viral expression and canula placement were used as exclusion
419 criteria for data analysis.

420

421 **In vivo photo-stimulation protocol**

422 Optical fiber implants were attached to optogenetics patch cables (M83L1, Thorlabs, UK)
423 connected to a rotary joint (Doric lenses) coupled to a 473-nm laser (Laserglow, Toronto,
424 Canada) controlled via TTL-USB interface with Arduino board. For feeding experiments, the

425 stimulation protocol was 1 s followed by 4 s break with 10ms light pulses with a frequency of
426 30Hz. For behavioral experiments, the stimulation protocol was 1 s followed by 0.5 s break
427 with 10ms light pulses with a frequency of 30Hz. We used 15mW of laser power to achieve
428 an irradiance of 5-10mW/mm^2 (PM100D, Thorlabs) on the target area following
429 https://web.stanford.edu/group/dlab/cgi-bin/graph/chart.php, above ChR2 threshold
430 activation (Lin et al., 2009).

431

432 **Food intake and body weight studies**

433 For food intake, body weight and metabolic parameters measurements, mice were single
434 housed and habituated in indirect calorimetry system cages for one week (Phenomaster, TSE
435 Systems, Germany). For acute ad libitum studies, access to food was removed in fed mice
436 2h before entering the dark cycle and CNO 1 mg/kg was i.p. administered 30 min before the
437 dark cycle onset when food was provided. For re-feeding studies, 12 hours dark cycle-food
438 deprived mice were i.p. injected with CNO at the beginning of the light cycle and 30 min after
439 food was provided. For subchronic studies, mice were i.p. injected twice a day (am and pm)
440 for 5 days with CNO following 5 days with saline.

441

442 **Behavioral tests**

443 For valence studies, mice were assessed in an adapted real-time place preference task
444 consisting in an open field arena with two connected identical chambers (30x25cm)
445 (D'Agostino et al., 2016; Kim et al., 2013; Stamatakis & Stuber, 2012), one of them paired
446 with optogenetic stimulation where mice were allowed free movement for 20 min. For anxiety
447 tests, mice were placed in an open arena (50x50cm) with virtual delimited central and
448 peripheral regions and allowed free movement for 10 minutes with and without stimulation in
449 different days. For anxiety and fear assessment, mice were placed in an elevated zero maze
450 (diameter 50cm, elevation 70 cm) with 2 hidden and 2 exposed zones and allowed free
451 movement between zones for 10 min. Tests were performed for each animal with and without
452 stimulation in different days. Time and locomotor parameters for each task and zone were
453 recorded using Any-Maze software (Stoelting, IL, USA).

454

455 **Immunohistochemistry and imaging**

456 All mice were injected with a terminal dose of anesthesia and transcardially perfused with
457 phosphate-buffered saline (PBS) followed by 10% neutral buffered formalin. Brains were
458 dissected, post-fixed 12 hours in formalin at 4°C, cryoprotected 48 hours with 30% sucrose
459 4°C and coronally sectioned in 5 series at 25 µm using a freezing microtome (8000, Bright
460 Instruments, UK). Sections were kept in protective anti-freeze solution at 4°C until they were
461 processed for immunohistochemistry as previously described (Yavari et al., 2016). Briefly,
462 NTS sections were washed with PBS-0.2% Tween20 30 min and then PBS (3x10 min),
463 blocked with 1%BSA/5%DS/0.25%Triton X-100 1 hour at room temperature and incubated
464 with primary antibody in blocking solution with anti-c-Fos (1:2500, 2250, CST, USA), anti- c-
465 Fos (for chromogenic) (1:5000, ABE457,Merck, UK), anti-mCherry (1:2000, AB0040-200,
466 Scigen, PT), anti-RFP (1:1000, 600-401-379, Rockland Immunochemicals, USA), anti-POMC
467 (1:3000, H-029-30, Phoenix Pharmaceuticals, USA), anti-hrGFP (1:2000, 240141, Agilent,
468 USA), anti-TH (1:2000, MAB318, Merck, Germany) 16 hours at room temperature. The next
469 day, sections were washed with PBS-Tween and PBS and incubated 1 hour with appropriate
470 secondary antibodies in blocking solution (1:500, AlexaFluor594, AlexaFluor488, Invitrogen,
471 UK) at room temperature. For c-Fos expression quantification in fast vs refed study,
472 chromogenic staining with DAB reagent was performed as previously described (D'Agostino
473 et al., 2016).

474 Images were acquired using Axioskope2 microscope and Axiovision software (Zeiss,
475 Germany). All images were converted to 8-bit, peudorecolored and cells counted using
476 ImageJ (Fiji).

477

478 **Electrophysiology**

479 *CRACM study*

480 CRACM experiments were performed as previously described (González et al., 2016). Six
481 *Vgat*^{Cre}:*Npy*^{hrGFP} mice and six *Vgat*^{Cre}:*Pomc*^{dsRed} mice bilaterally injected with AAV-ChR2-
482 mCherry and AAV-ChR2-mCherry respectively into the NTS, aged between 5 and 7 months
483 at the time of the electrophysiology experiments, were used. Expression of mCherry-ChR2
484 was targeted to NTS^{GABA} cells by stereotaxic injection of AAV as above. Coronal brain
485 sections 180-µm thick were prepared from these mice at least 8 days after virus injections

486 and were placed in a bath solution consisting of (in mM) 125 NaCl, 2.5 KCl, 1.2 NaH_2PO_4, 21
487 $NaHCO_3$, 1 glucose, 2 $MgCl_2$, 2 $CaCl_2$. GFP-expressing cells in the ARC were identified using
488 an upright microscope (Scientifica S-Scope-II) equipped with the appropriate fluorescence
489 filters. Whole-cell recordings from these cells were obtained with glass pipettes (World
490 Precision Instruments 1B150F-4) filled with a solution containing (in mM) 120 K-gluconate,
491 10 HEPES, 10 KCl, 1 EGTA, 2 MgCl2, 4K2ATP, and 1 Na2ATP, tip resistance 3-7 MOhm.
492 Data was acquired using Axon Instruments hardware (MultiClamp 700B, Digidata 1550). To
493 test for GABA inputs to AgRP/NPY^{ARC} cells, the membrane potential in these cells was
494 clamped at increasing levels of voltage (from -100 to -10 mV in 10-mV increments), while
495 ChR2-expressing terminals were stimulated by a single light pulse (CoolLED pE-4000) to
496 induce post-synaptic currents. Liquid junction potential, estimated to be 10 mV, was
497 subtracted from the measurements. Chloride equilibrium potential was calculated to be -60.3
498 mV.

499

500 *Sniffer-patch recordings*

501 Transverse hypothalamic slices from *$Vgat^{Cre}$:Npy^{hrGFP}* mice bilaterally injected AAV-DIO-
502 ChR2-mCherry were cut at 200-250 using a Leica VT1200S vibratome. Slices were incubated
503 for one hour in a solution containing (in mM): 124 NaCl, 3 KCl, 1 $CaCl_2$, 3 $MgCl_2$, 26 $NaHCO_3$,
504 1.25 NaH_2PO_4, 10 D-glucose, and bubbled with 95/5% O_2/CO_2, pH 7.4. After incubation,
505 slices were transferred to a recording chamber continuously superfused with an external
506 solution. The external solution composition differed from incubation solution in containing 2
507 mM $CaCl_2$ and 2 mM $MgCl_2$.

508 In all experiments the intracellular pipette solution for voltage-clamp recordings contained
509 (mM): 117.5 Cs-gluconate, 17.5 CsCl, 10 KOH-HEPES, 10 BAPTA, 8 NaCl, 5 QX-314, 2 Mg-
510 ATP, 0.3 GTP; for current-clamp recordings: 126 K-gluconate, 4 NaCl, 5 HEPES, 15 glucose,
511 1 $MgSO_4 \cdot 7H_2O$, 2 BAPTA, 3 Mg-ATP (pH 7.2, 295-310 mOsm in both cases); pipette
512 resistance was 7-9 MOhm; recordings were performed at 33-35ºC using Multiclamp-700B
513 amplifier with -60 or -70 mV holding current (for voltage-clamp recordings); signals were pre-
514 filtered and digitized at 10 kHz. In experiments where transmembrane currents were recorded
515 in outside-out patches only (sniffer-patch recordings), the $GABA_A$ receptors response was
516 isolated with a ligands cocktail containing 50 μM APV, 20 μM NBQX, 50 nM CGP-55845, 200
517 μM S-MCPG, 10 μM MDL-72222, and 1 μM strychnine.

518

519 **Statistics and data analysis**

520 Statistical analyses were performed using GraphPad Prism 9 software and are described in
521 the figure legend where 2-tail paired and unpaired Student t-test were used when comparing
522 2 groups and RM/two-way ANOVA test with Bonferroni post-hoc correction when comparing
523 4 groups. RNA-Seq data were analyzed as described above. No statistical method was used
524 to predefine sample size, randomization and blinding was performed for histological
525 quantifications. Statistical significance was accepted when the $p \leq 0.05$. Raw data was stored
526 in Excel and figures assembled with CorelVector and Affinity Designer software.

527

528 **Author Contributions**

529 The project was conceived by PBM and LKH. PBM designed and performed experiments
530 and analyzed data with assistance from YM; GKCD and GSHY performed and analyzed the
531 RNA-Seq data. SS and AG designed and performed electrophysiological recordings. The
532 manuscript was drafted by PBM with input from all other authors.

533

534 **Acknowledgements**

535 We gratefully acknowledge Dr F. Naneix for advice on optogenetics and editorial advice, and
536 staff within the University of Aberdeen Medical Research Facility and the Microscopy Facility
537 for their technical assistance. This work was supported by the ERC (MSCA-IF-NeuroEE-
538 660219) to PBM, Wellcome Trust Institutional Strategic Support Fund (204815/Z/16/Z) to
539 PBM and LKH, and the Biotechnology and Biological Sciences Research Council
540 (BB/V010557/1) to JAG and (BB/V016849/1) to LKH and SS. GKCD is funded by a BBSRC
541 CASE 4-year PhD studentship, co-funded by Novo Nordisk. GSHY is funded by the UK
542 Medical Research Council (MC_UU_00014/1).

543

544 **Conflict of interest**

545 The authors declare no competing financial interests.

Figure 1

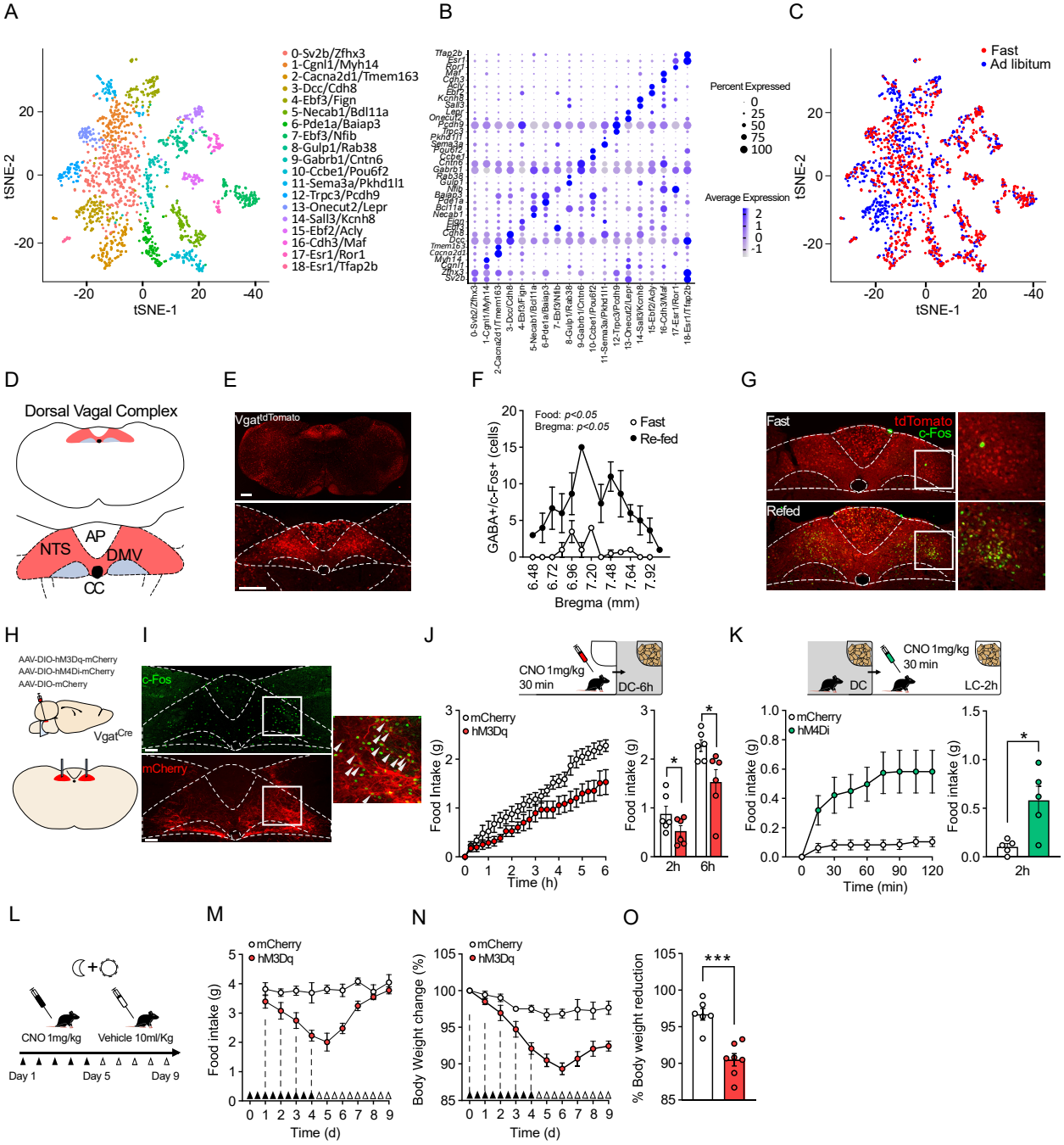
A
tSNE-2
tSNE-1
0-Sv2b/Zfhx3
1-Cgnl1/Myh14
2-Cacna2d1/Tmem163
3-Dcc/Cdh8
4-Ebf3/Fign
5-Necab1/Bdl11a
6-Pde1a/Baiap3
7-Ebf3/Nfib
8-Gulp1/Rab38
9-Gabrb1/Cntn6
10-Ccbe1/Pou6f2
11-Sema3a/Pkhd1l1
12-Trpc3/Pcdh9
13-Onecut2/Lepr
14-Sall3/Kcnh8
15-Ebf2/Acly
16-Cdh3/Maf
17-Esr1/Ror1
18-Esr1/Tfap2b
B
Percent Expressed
Average Expression
C
Fast
Ad libitum
D
Dorsal Vagal Complex
NTS
AP
DMV
CC
E
Vgat tdTomato
F
Food: p<0.05
Bregma: p<0.05
Fast
Re-fed
GABA+/c-Fos+ (cells)
Bregma (mm)
G
Fast
Refed
tdTomato
c-Fos
H
AAV-DIO-hM3Dq-mCherry
AAV-DIO-hM4Di-mCherry
AAV-DIO-mCherry
Vgat Cre
I
c-Fos
mCherry
J
CNO 1mg/kg
30 min
DC-6h
mCherry
hM3Dq
Food Intake (g)
Time (h)
Food intake (g)
2h
6h
K
CNO 1mg/kg
30 min
DC
LC-2h
mCherry
hM4Di
Food intake (g)
Time (min)
2h
L
CNO 1mg/kg
Vehicle 10ml/Kg
Day 1
Day 5
Day 9
M
mCherry
hM3Dq
Food intake (g)
Time (d)
N
mCherry
hM3Dq
Body Weight change (%)
Time (d)
O
% Body weight reduction

549 **Figure 2**

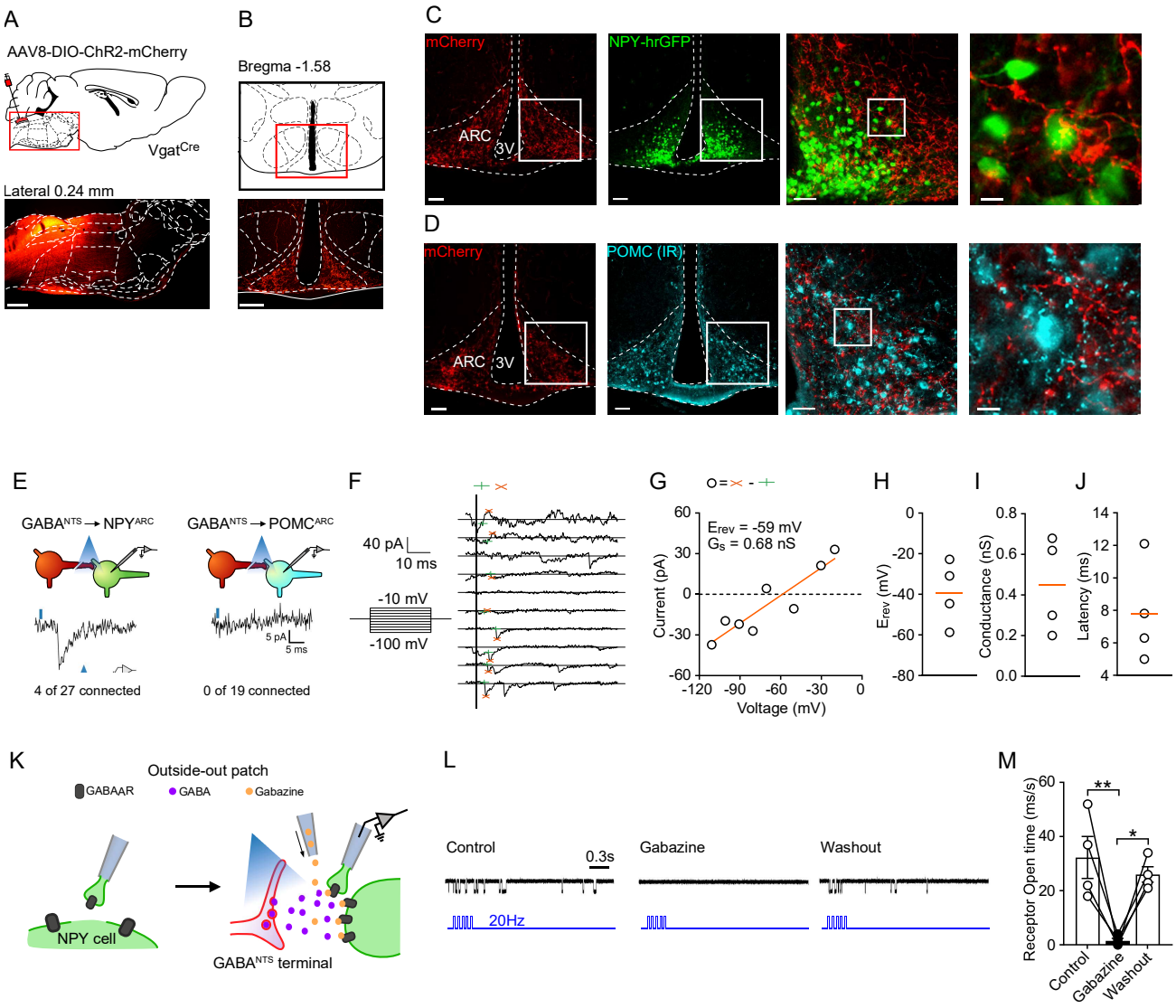

550

551

552 **Figure 3**

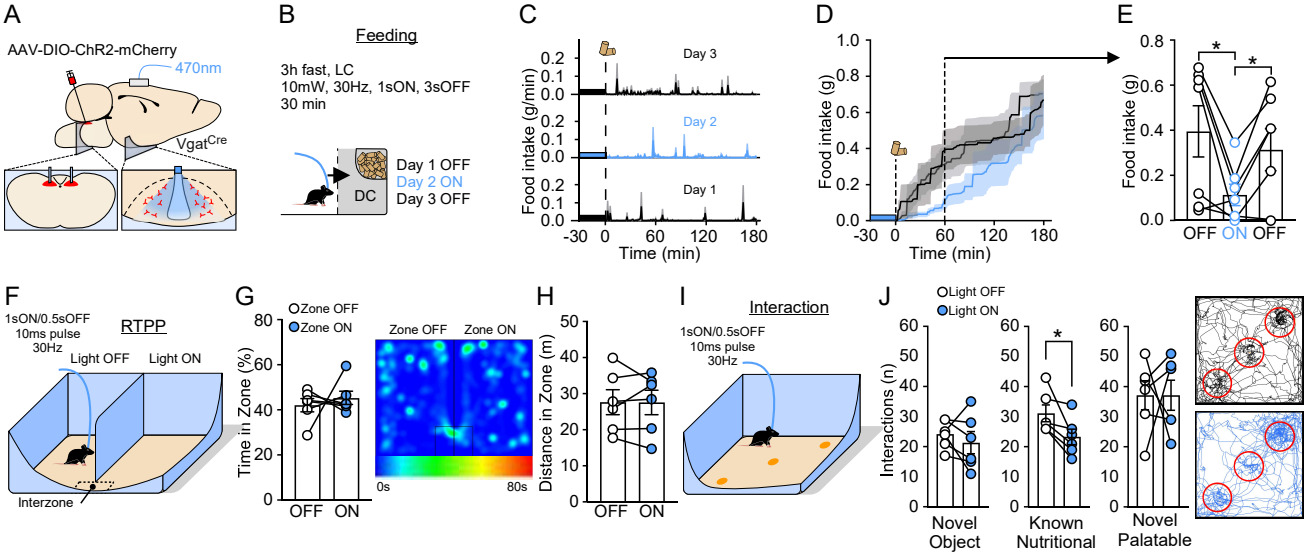

553

554

Figure 4

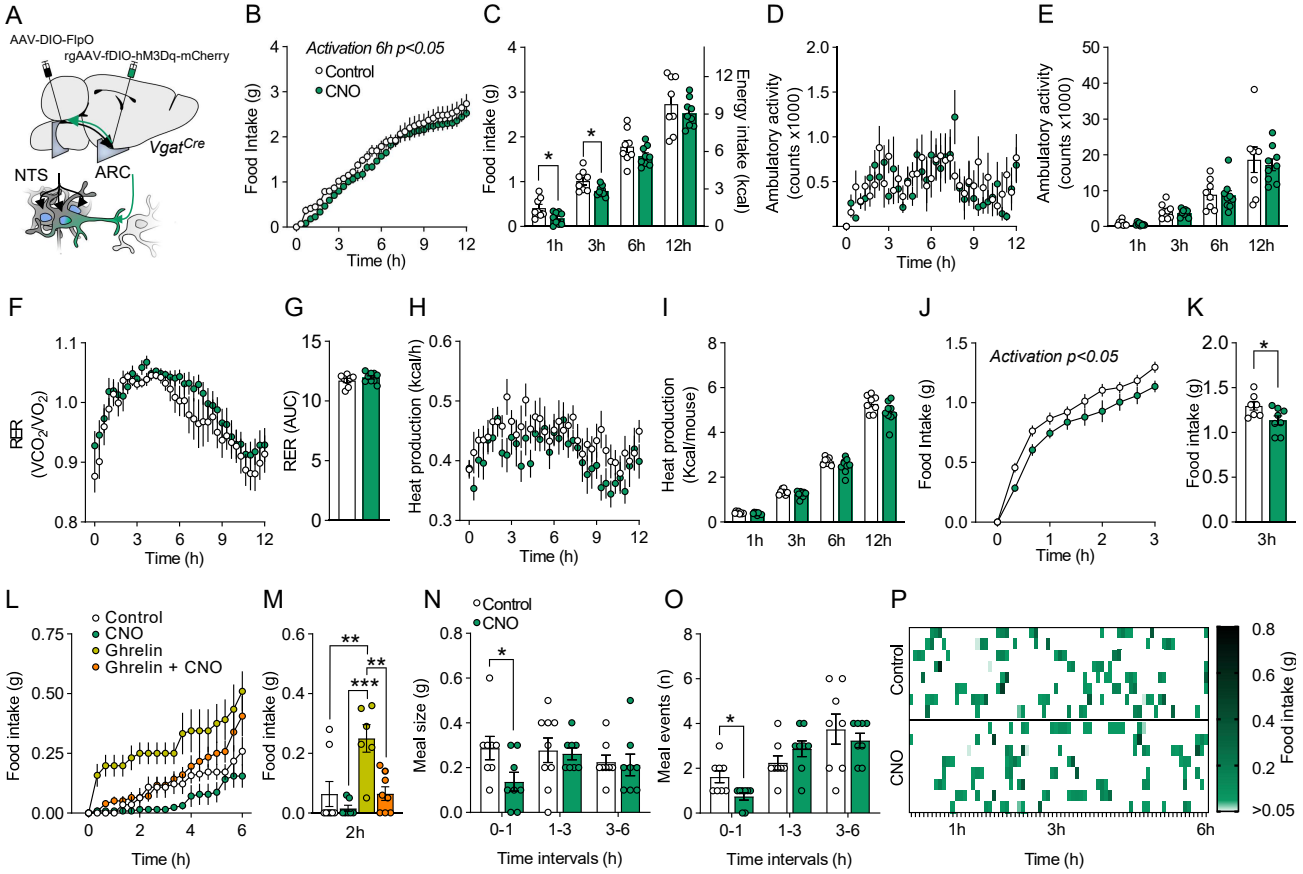
A
AAV-DIO-FlpO
rgAAV-fDIO-hM3Dq-mCherry
VgatCre
NTS
ARC
B
Activation 6h p<0.05
Control
CNO
Food Intake (g)
Time (h)
C
Food intake (g)
Energy intake (kcal)
1h
3h
6h
12h
D
Ambulatory activity (counts x1000)
Time (h)
E
Ambulatory activity (counts x1000)
F
RER (VCO2/VO2)
Time (h)
G
RER (AUC)
H
Heat production (kcal/h)
Time (h)
I
Heat production (Kcal/mouse)
J
Activation p<0.05
Food Intake (g)
Time (h)
K
Food intake (g)
3h
L
Control
CNO
Ghrelin
Ghrelin + CNO
Food intake (g)
Time (h)
M
Food intake (g)
2h
N
Control
CNO
Meal size (g)
0-1
1-3
3-6
Time intervals (h)
O
Meal events (n)
Time intervals (h)
P
Control
CNO
Food intake (g)
>0.05
1h
3h
6h
Time (h)

Supplementary Figure 1

A

Cluster-Gene	% Glp1r	% Gipr
18-Esr1/Tfap2b	0.00	0.00
17-Esr1/Ror1	0.00	0.00
16-Cdh3/Maf	4.08	10.20
15-Ebf2/Acly	3.77	1.89
14-Sall3/Kcnh8	3.51	0.00
13-Onecut2/Lepr	1.69	1.69
12-Trpc3/Pcdh9	0.00	0.00
11-Sema3a/Pkhd1l1	2.99	0.00
10-Ccbe1/Pou6f2	0.00	14.63
9-Gabrb1/Cntn6	3.26	2.17
8-Gulp1/Rab38	5.32	2.13
7-Ebf3/Nfib	0.00	1.82
6-Pde1a/Baiap3	0.91	2.73
5-Necab1/Bcl11a	0.89	0.89
4-Ebf3/Fign	1.79	0.89
3-Dcc/Cdh8	1.57	3.15
2-Cacna2d1/Tmem163	7.41	2.22
1-Cgnl1/Myh14	1.89	1.89
0-Sv2b/Zfhx3	2.82	3.10

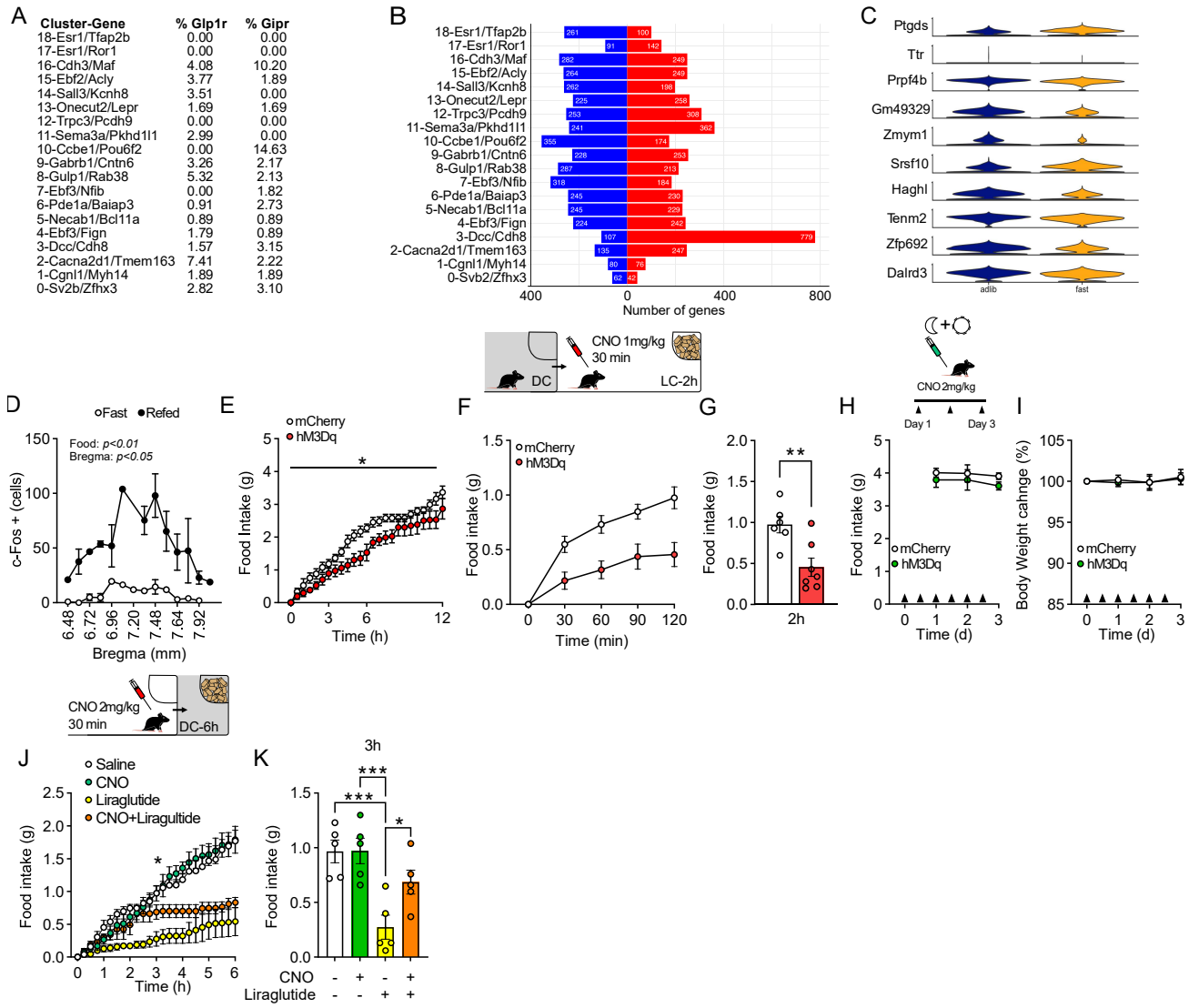

Supplementary Figure 2

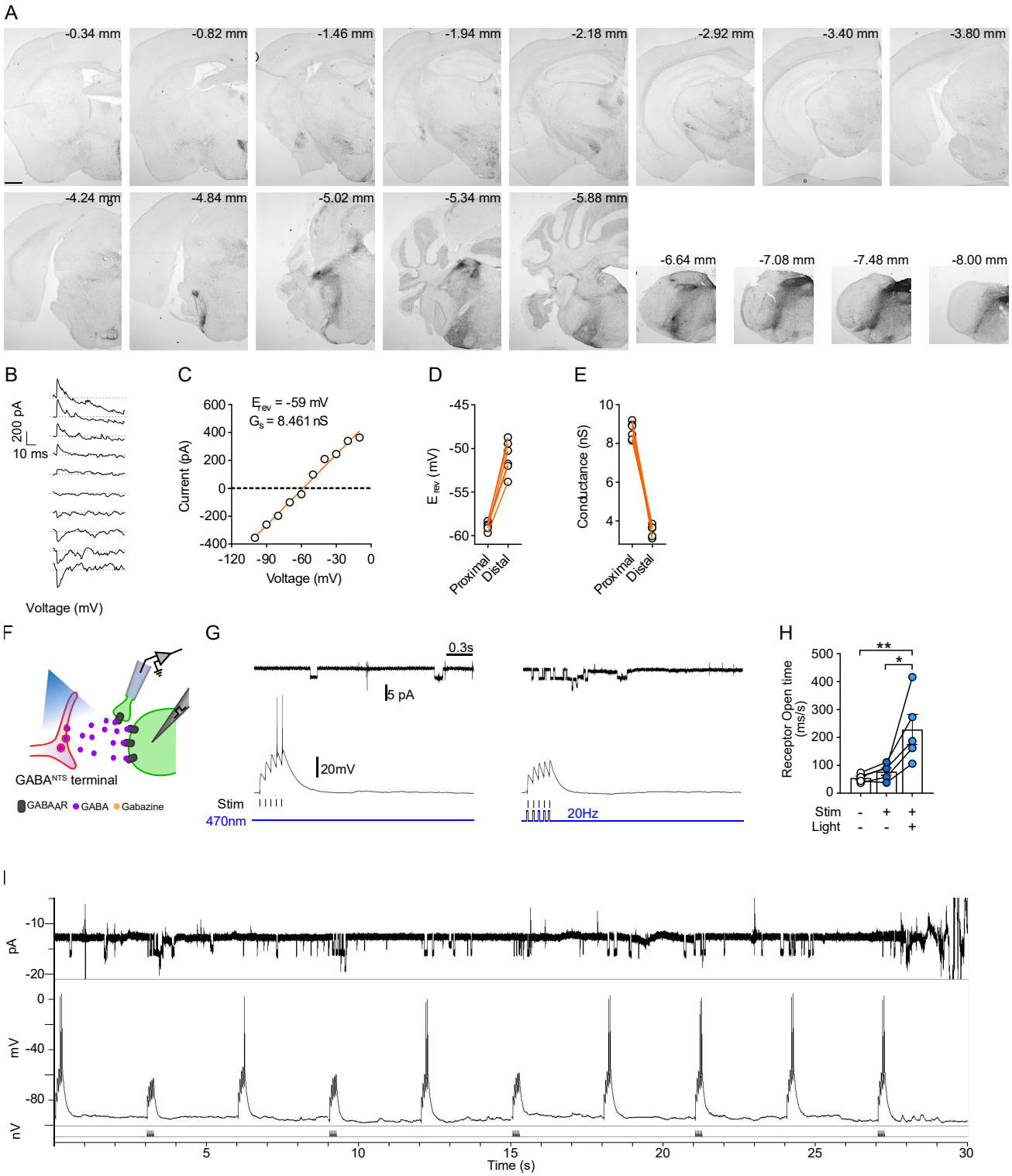

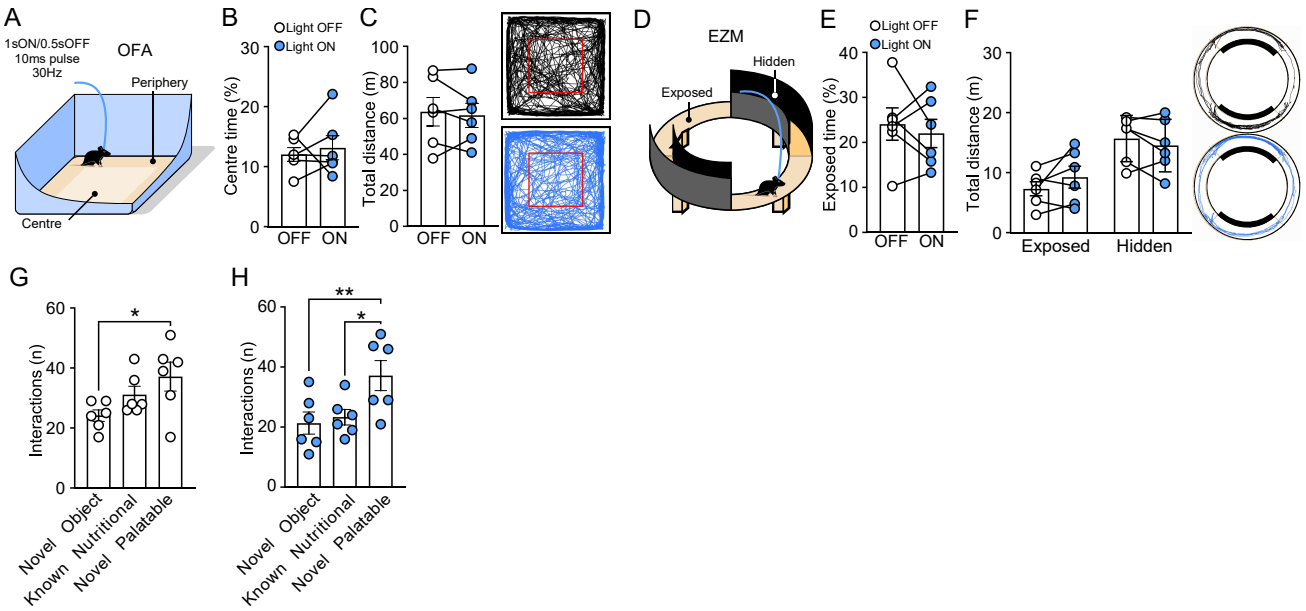
A
1sON/0.5sOFF
10ms pulse
30Hz
OFA
Periphery
Centre
B
Light OFF
Light ON
Centre time (%)
OFF ON
C
Total distance (m)
OFF ON
D
EZM
Hidden
Exposed
E
Light OFF
Light ON
Exposed time (%)
OFF ON
F
Total distance (m)
Exposed
Hidden
G
Interactions (n)
Novel Object
Known Nutritional
Novel Palatable
H
Interactions (n)
Novel Object
Known Nutritional
Novel Palatable

564

565

566 **Figures Legends**

567 **Figure 1. GABA^{NTS} activation reduces food intake and body weight.** (A) tSNE plot of
568 *Slc32a1*$^{+}$ neurons in the DVC colored by cluster, (B)Dot plot showing scaled expression of
569 marker genes for each of the 19 *Slc32a1*$^{+}$ clusters (C) tSNE plot of the *Slc32a1*$^{+}$ nuclei
570 colored by nutritional status (D) Schematic of the DVC (top) with zoom-in diagram showing
571 AP, NTS and DMC (bottom). (E) Representative photomicrograph of GABAergic cell
572 distribution in the medial brainstem (top) and in the DVC (bottom) using *Vgat*^{tdTom} mice. (F)
573 Quantification GABAergic cells expressing c-Fos following 16h fasting and fasting+2h
574 refeeding (n=3, Bregma level: two-way ANOVA $F_{(13,34)}$=2.63; p=0.012; Nutritional state: two-
575 way ANOVA $F_{(1,4)}$=8.69; p=0.042. (E) Representative micrograph of *Vgat*^{tdTom} cells (red)
576 expressing c-Fos (green) in mice fasted 16h (top) and re-fed for 2h (bottom). (H) Schematic
577 of AAV-DIO-hM3Dq/hM4Di/mCherry infused into NTS of *Vgat*^{Cre} mice. (I) Representative
578 photomicrograph of c-Fos (green) expression in hM3Dq-mCherry (red)-expressing cells in
579 the NTS of VgatCre mice treated with CNO (1 mg/kg, i.p) and (J) 6h cumulative and (J) 2h
580 and 6h total food intake (n=6, Unpaired t test $t_{(11)}$=2.663, p=0.0238) of GABA^{NTS}:hM3Dq CNO
581 injected mice compared to mCherry. (K) 2h cumulative and (J) 2h total food intake (n=5,
582 Unpaired t test $t_{(8)}$=3.205, p=0.0125) GABA^{NTS}:hM4Di CNO injected mice compared to
583 mCherry. (L) 10-day treatment protocol schematic. Daily CNO treatment significantly reduced
584 (M) food intake (RM two-way ANOVA $F_{(1,11)}$=20.57; P=0.0008), (N) body weight (n=6/7, RM
585 two-way ANOVA ($F_{(1,11)}$=21.96; p=0.0007) and (O) body weight change GABA$^{NTS:hM3Dq}$ mice
586 compared to control GABA^{NTS}:mCherry mice (n=6/7, Unpaired t test $t_{(11)}$=5.252, p=0.0003).
587 C-D n=4/group, H-K n=6; M-O n=6 mCherry and n=7 hM3Dq. Data represented as
588 mean±S.E.M. *: p<0.05; **: p<0.01; ***: p<0.001. AP: Area Postrema; CC: Centre canal;
589 DMV: Doral motor nucleus of the vagus nerve; NTS: Nucleus of the solitary tract.

590 **Figure 2. GABA^{NTS} projections to the ARC release GABA into AgRP/NPY neurons.** (A)
591 Illustration depicting details for NTS injection of AAV-DIO-ChR2-mCherry (top) and
592 representative photomicrograph (scale 1mm) of injection (bottom) in *Vgat^{Cre}* mice and (B)
593 ChR2-mcherry containing fibers in the ARC (scale 200um). (B) Representative
594 photomicrographs (scale 100um) and magnification (scale 50 and 10um) ChR2-mCherry
595 fibers in the ARC close to NPY^{hrGFP}-expressing cells and (D) POMC-expressing cells and in
596 *Vgat^{Cre}* mice bilaterally injected AAV-DIO-ChR2-mCherry. (E-J) *Vgat^{Cre}:Npy^{hrGFP}* mice
597 CRACM study. (E) Representative membrane potential response of NPYGFP and
598 POMCDsRed cells after light stimulation of mCherry containing terminals. (F) Representative
599 membrane current in Npy^{hrGFP} cell recorded during a voltage-clamp experiment from -100mV
600 to -10mV in 10-mV steps. (Vertical line: light pulse; green cross: base line; red cross: peak
601 value). (G) Representative light-induced post-synaptic current during voltage clamp
602 experiment showing peak conductance, G_s, and reversal potential, E_{rev}. (H) Individual values
603 and median of (H) E_{rev}, (I) Conductance, G_s and (I) latency of all responsive cells. (K)
604 Diagram of outside-out patch technique in *Vgat^{Cre}:Npy^{hrGFP}* mice bilaterally injected AAV-DIO-
605 ChR2-mCherry. (L) Representative channel opening recordings of control (left) gabazine
606 (middle) and washout (right) recordings. (M) Quantification of receptor opening time (n=4,
607 RM two-way ANOVA $F_{(2,6)}$=16.14; p=0.0039, Bonferroni adjusted p=0.0051 Control vs
608 Gabazine and p=0.0156 Gabazine vs Washout. Data in M are expressed as mean±S.E.M.
609 E-J: 4/27 cells NPYhrGFP and 0/19 cells POMCdsRed; K-M: n=4-5 patches. *: p<0.05; **:
610 p<0.01.

611 **Figure 3. Activation of GABA^{NTS}→ARC projections reduces food intake without**
612 **inducing aversion**. (A) Schematic of viral infection and optic fiber placement for in vivo
613 stimulation of GABA^{NTS}→ARC. (B) Protocol of stimulation. (C) Representative 1min
614 resolution time plot of 3h food intake measurement. GABA^{NTS}→ARC stimulation significantly
615 reduces (D) cumulative 3h food intake and (E) 60min intake (n=7, day 1 (OFF) vs day 2 (ON)
616 paired Student t-test $t_{(6)}$=3.035, p=0.0229; day 2 (ON) vs day 3 (OFF) paired Student t-test
617 $t_{(6)}$=3.283, p=0.0168). (F) Diagram illustrating RTPP task. GABA^{NTS}→ARC does not alter (G)
618 time spent (representative heat map of time) or (H) distance travelled in stimulated and non-
619 stimulated zones. (I) Diagram illustrating an object interaction task. (J) Interactions with novel,
620 known nutritional or novel palatable objects and a representative path track around each
621 object (red circle). GABA^{NTS}→ARC stimulation reduced interaction with known nutritional item
622 (n=6, Student's t test $t_{(5)}$=3.043, p=0.0287). Data are expressed as individual values and as
623 mean±S.E.M, n=6 mice. *: p<0.05; RTPP: real-time place preference.

624 **Figure 4. Chemogenetic activation of GABA^{NTS}→ARC neurons induces satiety**. (A)
625 Diagram illustrating the two-virus intersectional strategy to express hM3Dq only in GABA^{NTS}
626 neurons projecting to the ARC. Mice were treated with saline or CNO (1 mg/kg, i.p.). (B) CNO
627 significantly reduced cumulative food intake over 6h (0-6h $F_{(1,15)}$=7.418, p=0.0157), (C) 1h
628 (Unpaired t-test $t_{(15)}$=2.648, p=0.0183) and 3h (Unpaired t-test, $t_{(15)}$=2.568 P=0.0214) food
629 intake compared to saline. (D) CNO did not alter 12h or (E) 1, 3, 6 or 12h quantification of
630 ambulation; (F) 12h RER or (G) AUC quantification; (H) 12h or (I) 1, 3, 6 and 12h heat
631 production per mouse compared to saline. (J-K) CNO significantly reduced 3h food intake
632 following overnight fasting (J, 2-way ANOVA $F_{(1.13)}$=6.139, p=0.0277 and K, unpaired t-test
633 $t_{(13)}$=2.320, p=0.0372). (L-M) CNO attenuated ghrelin hyperphagia over 2h (RM ANOVA
634 $F_{(3,16)}$=11.12; p=0.0003, Bonferroni adjusted p=0.0042 control vs ghrelin, p=0.0003 CNO vs
635 ghrelin and p=0.002 Ghrelin vs Ghrelin+CNO). (N) CNO reduced meal size (Unpaired t-test,
636 $t_{(14)}$=2.256, p=0.0406) and (O-P) decreased meal number (Unpaired t-test, t(14)=2.824,
637 p=0.0135) compared to control. Data are expressed as individual values and as mean±SEM.
638 *: p<0.05; **: p<0.01. ***: p<0.001.

639

640 **Supplementary Figure 1**

641 (A) Proportion of GLP1-R and GIPR expression in each *Slc32a1*$^{+}$ cluster (B) Number of genes
642 upregulated (red) and downregulated (blue) in response to an overnight fast in each cluster.
643 Genes included were significantly differentially regulated ($P < 0.05$). (C) Top 10 genes
644 differentially expressed in ad libitum vs fasting in *Slc32a1*$^{+}$ neurons (D) Quantification of total
645 NTS c-Fos-expressing cells following 16h fasting and fasting+2h refeeding (n=3, Bregma
646 level: two-way ANOVA $F_{(13,34)}=3.16$; p=0.004; Nutritional state: two-way ANOVA $F_{(1,4)}=18.61$;
647 P=0.012). (E) 12h dark cycle food intake in hM3Dq vs mCherry mice injected with CNO. (F)
648 Food intake following an overnight fast compared to mCherry in GABA^{NTS}:hM3Dq mice (n=6,
649 RM two-way ANOVA $F_{(1,11)}=10.97$; P=0.0069) and (G) 2h food intake (n=6/7, Unpaired t test,
650 $t_{(11)}=3.392$ p=0.006). (G-I) Food intake and body weight change in hM4Di vs mCherry mice
651 twice daily injected with CNO (2mg/Kg). (J-K) Food intake in hM4Di mice co-administered
652 with CNO and Liraglutide (RM: ANOVA $F_{(3,12)}=15.64$; P=0.002, Bonferroni adjusted p=0.0004
653 Saline vs Liraglutide, P=0.0004 CNO vs Liraglutide and P=0.0263 Liraglutide vs
654 Liraglutide+CNO).

655

656

657 **Figure S2. GABA^{NTS} projection pattern and CRACM additional analysis**. (A)
658 Representative photomicrographs (scale 100µm) of ChR2-mCherry fibers in a serial rostro-
659 caudal distribution of a *Vgat*^{Cre} mouse brain injected with AAV-DIO-ChR2-mCherry into the
660 NTS. (B-E) A simulated voltage-clamp experiment in an anatomically realistic model of a
661 medium spiny neuron, using the same voltage steps as those described for electrophysiology
662 experiments (Figure 2E-G). The effect of optogenetic stimulation was modelled as a single
663 GABAergic event taking place at each step. (C) Current amplitude was plotted against
664 voltage (as in Figure 2E-G), and a linear fit was used to estimate peak conductance G_s and
665 reversal potential E_{rev}. (D-E) Simulated optogenetic activation of GABA inputs making
666 synaptic contact only on dendrites close to the soma ("prox.", proximal dendrites) was
667 compared to the same type of activation of GABA synapses connected only to dendrites far
668 from the soma ("distal" dendrites) in six different medium spiny neuron models. The reversal
669 potential for GABA in the model was set to -60 mV, and this is close to what was measured
670 at the soma when GABA synaptic inputs were located on dendrites close to the soma.
671 However, when GABA synapses were activated only on dendrites distant from the soma E_{rev},
672 was more positive than expected and conductance G_s was attenuated. (F) Diagram of

673 outside-out patch technique coupled to a postsynaptic electrical stimulator. (G, left)
674 Representative response of Npy^{hrGFP} cell subjected to series of five electrical stimuli, each
675 evoking excitatory post-synaptic potential (EPSP) of sub-threshold amplitude and (G, right)
676 same cell with electrical stimuli coupled with 470nm light burst. (M) Quantification of receptor
677 opening time (n=5, two-way RM ANOVA $F_{(2,8)}$=11.28; p=0.0047, Bonferroni adjusted
678 P=0.0072 NS vs SL and P=0.0157 S vs SL), L-M n=4-5 cells. (I) Representative response of
679 a single Npy^{hrGFP} cell subjected to 10 series of five electrical stimuli, each evoking excitatory
680 post-synaptic potential (EPSP) of sub-threshold amplitude coupled with 470nm light burst in
681 *$Vgat^{Cre}$::NPY^{hrGFP}* mouse injected with AAV-DIO-ChR2-mCherry into the NTS. NS: No
682 stimulation; S: Stimulation; SL: Stimulation+Light.
683
684

685 **Figure S3. Optogenetic activation of GABA^{NTS}→ARC in *Vgat^{Cre}* mice does not induce**
686 **anxiety-like behavior**. (A) Diagram illustrating open field arena (OFA) task. GABA^{NTS}→ARC
687 does not alter (B) time spent in the center or (C) distance travelled (representative trace of
688 the movement) during the test. (D) Diagram illustrating elevated zero maze (EZM) task.
689 GABA^{NTS}→ARC does not alter (E) time spent in the exposed area or (F) distance travelled in
690 each zone (representative trace of the movement) during the test. (G-H) Quantification of
691 number of interactions with a novel object, a known nutritional food item or a novel palatable
692 food item in mice (G) non-stimulated (RM ANOVA ($F_{(2,10)}$=4.993; p=0.0314, Bonferroni
693 adjusted p=0.0306 NO vs NP) and (H) stimulated (RM ANOVA $F_{(2,10)}$=10.71; p=0.0033,
694 Bonferroni adjusted p=0.0051 NO vs NP; p=0.0121 KN vs NP). Data are expressed as
695 individual values and as mean±S.E.M, n=6 mice. *:p<0.05; **:p<0.01. NO: novel object; NP:
696 novel palatable; KN: known nutritional.

697 **REFERENCES**

698 Aklan, I., Sayar Atasoy, N., Yavuz, Y., Ates, T., Coban, I., Koksalar, F., Filiz, G., Topcu, I. C.,
699 Oncul, M., Dilsiz, P., Cebecioglu, U., Alp, M. I., Yilmaz, B., Davis, D. R., Hajdukiewicz,
700 K., Saito, K., Konopka, W., Cui, H., & Atasoy, D. (2020). NTS Catecholamine Neurons
701 Mediate Hypoglycemic Hunger via Medial Hypothalamic Feeding Pathways. *Cell*
702 *Metabolism*, *31*(2), 313-326.e5. https://doi.org/10.1016/j.cmet.2019.11.016

703 Alexander, G. M., Rogan, S. C., Abbas, A. I., Armbruster, B. N., Pei, Y., Allen, J. A.,
704 Nonneman, R. J., Hartmann, J., Moy, S. S., Nicolelis, M. A., McNamara, J. O., & Roth,
705 B. L. (2009). Remote control of neuronal activity in transgenic mice expressing evolved
706 G protein-coupled receptors. *Neuron*, *63*(1), 27–39.
707 https://doi.org/10.1016/J.NEURON.2009.06.014

708 Alhadeff, A. L., Mergler, B. D., Zimmer, D. J., Turner, C. A., Reiner, D. J., Schmidt, H. D.,
709 Grill, H. J., & Hayes, M. R. (2017). Endogenous Glucagon-like Peptide-1 Receptor
710 Signaling in the Nucleus Tractus Solitarius is Required for Food Intake Control.
711 *Neuropsychopharmacology : Official Publication of the American College of*
712 *Neuropsychopharmacology*, *42*(7), 1471–1479. https://doi.org/10.1038/NPP.2016.246

713 Andermann, M. L., & Lowell, B. B. (2017). Toward a Wiring Diagram Understanding of
714 Appetite Control. *Neuron*, *95*(4), 757–778.
715 https://doi.org/10.1016/J.NEURON.2017.06.014

716 Aponte, Y., Atasoy, D., & Sternson, S. M. (2011). AGRP neurons are sufficient to orchestrate
717 feeding behavior rapidly and without training. *Nature Neuroscience*, *14*(3), 351–355.
718 https://doi.org/10.1038/NN.2739

719 Berridge, K. C. (2004). Motivation concepts in behavioral neuroscience. *Physiology and*
720 *Behavior*, *81*(2), 179–209. https://doi.org/10.1016/j.physbeh.2004.02.004

721 Berrios, J., Li, C., Madara, J. C., Garfield, A. S., Steger, J. S., Krashes, M. J., & Lowell, B. B.
722 (2021). Food cue regulation of AGRP hunger neurons guides learning. *Nature*, *595*, 695.
723 https://doi.org/10.1038/s41586-021-03729-3

724 Betley, J. N., Cao, Z. F. H., Ritola, K. D., & Sternson, S. M. (2013). Parallel, Redundant Circuit
725 Organization for Homeostatic Control of Feeding Behavior. *Cell*, *155*(6), 1337–1350.
726 https://doi.org/10.1016/J.CELL.2013.11.002

Betley, J. N., Xu, S., Cao, Z. F. H., Gong, R., Magnus, C. J., Yu, Y., & Sternson, S. M. (2015). Neurons for hunger and thirst transmit a negative-valence teaching signal. *Nature*, *521*(7551), 180. https://doi.org/10.1038/NATURE14416

Blevins, J. E., Schwartz, M. W., & Baskin, D. G. (2004). Evidence that paraventricular nucleus oxytocin neurons link hypothalamic leptin action to caudal brain stem nuclei controlling meal size. *American Journal of Physiology - Regulatory Integrative and Comparative Physiology*, *287*(1 56-1), 87–96. https://doi.org/10.1152/AJPREGU.00604.2003/ASSET/IMAGES/LARGE/ZH600704225 10005.JPEG

Campos, A., Port, J. D., & Acosta, A. (2022). Integrative Hedonic and Homeostatic Food Intake Regulation by the Central Nervous System: Insights from Neuroimaging. In *Brain Sciences* (Vol. 12, Issue 4). MDPI. https://doi.org/10.3390/brainsci12040431

Chen, H. Y., Trumbauer, M. E., Chen, A. S., Weingarth, D. T., Adams, J. R., Frazier, E. G., Shen, Z., Marsh, D. J., Feighner, S. D., Guan, X. M., Ye, Z., Nargund, R. P., Smith, R. G., van der Ploeg, L. H. T., Howard, A. D., Macneil, D. J., & Qian, S. (2004). Orexigenic Action of Peripheral Ghrelin Is Mediated by Neuropeptide Y and Agouti-Related Protein. *Endocrinology*, *145*(6), 2607–2612. https://doi.org/10.1210/EN.2003-1596

Chen, J., Cheng, M., Wang, L., Zhang, L., Xu, D., Cao, P., Wang, F., Herzog, H., Song, S., & Zhan, C. (2020). A Vagal-NTS Neural Pathway that Stimulates Feeding. *Current Biology*, *30*(20), 3986-3998.e5. https://doi.org/10.1016/J.CUB.2020.07.084

Cheng, W., Gordian, D., Ludwig, M. Q., Pers, T. H., Seeley, R. J., & Myers, M. G. (2022). Hindbrain circuits in the control of eating behaviour and energy balance. *Nature Metabolism*, *4*(7), 826–835. https://doi.org/10.1038/s42255-022-00606-9

Cheng, W., Ndoka, E., Hutch, C., Roelofs, K., MacKinnon, A., Khoury, B., Magrisso, J., Kim, K. S., Rhodes, C. J., Olson, D. P., Seeley, R. J., Sandoval, D., & Myers, M. G. (2020). Leptin receptor-expressing nucleus tractus solitarius neurons suppress food intake independently of GLP1 in mice. *JCI Insight*, *5*(7). https://doi.org/10.1172/JCI.INSIGHT.134359

Clifton, P. G. (2000). Meal patterning in rodents: psychopharmacological and neuroanatomical studies. *Neuroscience & Biobehavioral Reviews*, *24*(2), 213–222. https://doi.org/10.1016/S0149-7634(99)00074-3

758 Cork, S. C., Richards, J. E., Holt, M. K., Gribble, F. M., Reimann, F., & Trapp, S. (2015).
759 Distribution and characterisation of Glucagon-like peptide-1 receptor expressing cells in
760 the mouse brain. *Molecular Metabolism*, *4*(10), 718–731.
761 https://doi.org/10.1016/j.molmet.2015.07.008

762 Cummings, D. E., Purnell, J. Q., Frayo, R. S., Schmidova, K., Wisse, B. E., & Weigle, D. S.
763 (2001). A Preprandial Rise in Plasma Ghrelin Levels Suggests a Role in Meal Initiation
764 in Humans. *Diabetes*, *50*(8), 1714–1719. https://doi.org/10.2337/DIABETES.50.8.1714

765 D'Agostino, G., & Luckman, S. M. (2022). Brainstem peptides and peptidergic neurons in the
766 regulation of appetite. *Current Opinion in Endocrine and Metabolic Research*, *24*,
767 100339. https://doi.org/10.1016/J.COEMR.2022.100339

768 D'Agostino, G., Lyons, D., Cristiano, C., Lettieri, M., Olarte-Sanchez, C., Burke, L. K.,
769 Greenwald-Yarnell, M., Cansell, C., Doslikova, B., Georgescu, T., Martinez de Morentin,
770 P. B., Myers, M. G., Rochford, J. J., & Heisler, L. K. (2018). Nucleus of the Solitary Tract
771 Serotonin 5-HT2C Receptors Modulate Food Intake. *Cell Metabolism*, *28*(4), 619-
772 630.e5. https://doi.org/10.1016/J.CMET.2018.07.017

773 D'Agostino, G., Lyons, D. J., Cristiano, C., Burke, L. K., Madara, J. C., Campbell, J. N.,
774 Garcia, A. P., Land, B. B., Lowell, B. B., Dileone, R. J., & Heisler, L. K. (2016). Appetite
775 controlled by a cholecystokinin nucleus of the solitary tract to hypothalamus neurocircuit.
776 *ELife*, *5*. https://doi.org/10.7554/eLife.12225

777 Deem, J. D., Faber, C. L., & Morton, G. J. (2022). AgRP neurons: Regulators of feeding,
778 energy expenditure, and behavior. *FEBS Journal*, *289*(8), 2362–2381.
779 https://doi.org/10.1111/FEBS.16176

780 Dietrich, M. O., Bober, J., Ferreira, J. G., Tellez, L. A., Mineur, Y. S., Souza, D. O., Gao, X.-
781 B., Picciotto, M. R., Araújo, I., Liu, Z.-W., & Horvath, T. L. (2012). AgRP neurons regulate
782 development of dopamine neuronal plasticity and nonfood-associated behaviors. *Nature*
783 *Neuroscience*. https://doi.org/10.1038/nn.3147

784 Dietrich, M. O., Zimmer, M. R., Bober, J., & Horvath, T. L. (2015). Hypothalamic Agrp Neurons
785 Drive Stereotypic Behaviors beyond Feeding. *Cell*, *160*(6), 1222–1232.
786 https://doi.org/10.1016/J.CELL.2015.02.024

787 Dowsett, G. K. C., Lam, B. Y. H., Tadross, J. A., Cimino, I., Rimmington, D., Coll, A. P., Polex-
788 Wolf, J., Knudsen, L. B., Pyke, C., & Yeo, G. S. H. (2021). A survey of the mouse
789 hindbrain in the fed and fasted states using single-nucleus RNA sequencing. *Molecular*
790 *Metabolism*, *53*, 101240. https://doi.org/10.1016/J.MOLMET.2021.101240

791 Fenno, L. E., Mattis, J., Ramakrishnan, C., & Deisseroth, K. (2017). A Guide to Creating and
792 Testing New INTRSECT Constructs. *Current Protocols in Neuroscience*, *80*(1), 4.39.1-
793 4.39.24. https://doi.org/10.1002/CPNS.30

794 Fenno, L. E., Mattis, J., Ramakrishnan, C., Hyun, M., Lee, S. Y., He, M., Tucciarone, J.,
795 Selimbeyoglu, A., Berndt, A., Grosenick, L., Zalocusky, K. A., Bernstein, H., Swanson,
796 H., Perry, C., Diester, I., Boyce, F. M., Bass, C. E., Neve, R., Huang, Z. J., & Deisseroth,
797 K. (2014). Targeting cells with single vectors using multiple-feature Boolean logic. *Nature*
798 *Methods*, *11*(7), 763–772. https://doi.org/10.1038/nmeth.2996

799 Fortin, S. M., Lipsky, R. K., Lhamo, R., Chen, J., Kim, E., Borner, T., Schmidt, H. D., & Hayes,
800 M. R. (2020). GABA neurons in the nucleus tractus solitarius express GLP-1 receptors
801 and mediate anorectic effects of liraglutide in rats HHS Public Access. *Sci Transl Med*,
802 *12*(533), 109–114. https://doi.org/10.1126/scitranslmed.aay8071

803 Garau, C., Blomeley, C., Burdakov, D., & Burdakov, D. (2020). Orexin neurons and inhibitory
804 Agrp→orexin circuits guide spatial exploration in mice. *The Journal of Physiology*, *598*,
805 4371–4383. https://doi.org/10.1113/JP280158

806 Georgescu, T., Lyons, D., Doslikova, B., Garcia, A. P., Marston, O., Burke, L. K., Chianese,
807 R., Lam, B. Y. H., Yeo, G. S. H., Rochford, J. J., Garfield, A. S., & Heisler, L. K. (2020).
808 Neurochemical Characterization of Brainstem Pro-Opiomelanocortin Cells.
809 *Endocrinology*, *161*(4). https://doi.org/10.1210/endocr/bqaa032

810 González, J. A., Iordanidou, P., Strom, M., Adamantidis, A., & Burdakov, D. (2016). Awake
811 dynamics and brain-wide direct inputs of hypothalamic MCH and orexin networks. *Nature*
812 *Communications*, *7*. https://doi.org/10.1038/NCOMMS11395

813 Graham, D. L., Durai, H. H., Trammell, T. S., Noble, B. L., Mortlock, D. P., Galli, A., &
814 Stanwood, G. D. (2020). A novel mouse model of glucagon-like peptide-1 receptor
815 expression: A look at the brain. *Journal of Comparative Neurology*, *528*(14), 2445–2470.
816 https://doi.org/10.1002/cne.24905

817 Grill, H. J., & Hayes, M. R. (2012). Hindbrain Neurons as an Essential Hub in the
818 Neuroanatomically Distributed Control of Energy Balance. *Cell Metabolism*, *16*(3), 296–
819 309. https://doi.org/10.1016/J.CMET.2012.06.015

820 Hahn, T. M., Breininger, J. F., Baskin, D. G., & Schwartz, M. W. (1998). Coexpression of Agrp
821 and NPY in fasting-activated hypothalamic neurons. *Nature Neuroscience 1998 1:4*,
822 *1*(4), 271–272. https://doi.org/10.1038/1082

823 Han, Y., Xia, G., Srisai, D., Meng, F., He, Y., Ran, Y., He, Y., Farias, M., Hoang, G., Tóth, I.,
824 Dietrich, M. O., Chen, M. H., Xu, Y., & Wu, Q. (2021). Deciphering an AgRP-
825 serotoninergic neural circuit in distinct control of energy metabolism from feeding. *Nature*
826 *Communications 2021 12:1*, *12*(1), 1–16. https://doi.org/10.1038/s41467-021-23846-x

827 Hao, Y., Hao, S., Andersen-Nissen, E., Mauck, W. M., Zheng, S., Butler, A., Lee, M. J., Wilk,
828 A. J., Darby, C., Zager, M., Hoffman, P., Stoeckius, M., Papalexi, E., Mimitou, E. P., Jain,
829 J., Srivastava, A., Stuart, T., Fleming, L. M., Yeung, B., … Satija, R. (2021). Integrated
830 analysis of multimodal single-cell data. *Cell*, *184*(13), 3573-3587.e29.
831 https://doi.org/10.1016/j.cell.2021.04.048

832 Heinz, D. E., Schöttle, V. A., Nemcova, P., Binder, F. P., Ebert, T., Domschke, K., & Wotjak,
833 C. T. (2021). Exploratory drive, fear, and anxiety are dissociable and independent
834 components in foraging mice. *Translational Psychiatry 2021 11:1*, *11*(1), 1–12.
835 https://doi.org/10.1038/s41398-021-01458-9

836 Heisler, L. K., Jobst, E. E., Sutton, G. M., Zhou, L., Borok, E., Thornton-Jones, Z., Liu, H. Y.,
837 Zigman, J. M., Balthasar, N., Kishi, T., Lee, C. E., Aschkenasi, C. J., Zhang, C. Y., Yu,
838 J., Boss, O., Mountjoy, K. G., Clifton, P. G., Lowell, B. B., Friedman, J. M., … Cowley,
839 M. A. (2006). Serotonin Reciprocally Regulates Melanocortin Neurons to Modulate Food
840 Intake. *Neuron*, *51*(2), 239–249. https://doi.org/10.1016/j.neuron.2006.06.004

841 Heisler, L. K., & Lam, D. D. (2017). An appetite for life: brain regulation of hunger and satiety.
842 *Current Opinion in Pharmacology*, *37*, 100–106.
843 https://doi.org/10.1016/J.COPH.2017.09.002

844 Hentges, S. T., Otero-Corchon, V., Pennock, R. L., King, C. M., & Low, M. J. (2009).
845 Proopiomelanocortin Expression in both GABA and Glutamate Neurons. *The Journal of*
846 *Neuroscience*, *29*(43), 13684–13690. https://doi.org/10.1523/JNEUROSCI.3770-
847 09.2009

848 Holt, M. K., Richards, J. E., Cook, D. R., Brierley, D. I., Williams, D. L., Reimann, F., Gribble,
849 F. M., & Trapp, S. (2019). Preproglucagon neurons in the nucleus of the solitary tract are
850 the main source of brain GLP-1, mediate stress-induced hypophagia, and limit unusually
851 large intakes of food. *Diabetes*, *68*(1), 21–33. https://doi.org/10.2337/DB18-0729/-/DC1

852 Hyun, U., & Sohn, J. W. (2022). Autonomic control of energy balance and glucose
853 homeostasis. *Experimental & Molecular Medicine 2022 54:4*, *54*(4), 370–376.
854 https://doi.org/10.1038/s12276-021-00705-9

855 Jensen, C. B., Pyke, C., Rasch, M. G., Dahl, A. B., Knudsen, L. B., & Secher, A. (2018).
856 Characterization of the Glucagonlike Peptide-1 Receptor in Male Mouse Brain Using a
857 Novel Antibody and In Situ Hybridization. *Endocrinology*, *159*(2), 665–675.
858 https://doi.org/10.1210/en.2017-00812

859 Jikomes, N., Ramesh, R. N., Mandelblat-Cerf, Y., & Andermann, M. L. (2016). Preemptive
860 Stimulation of AgRP Neurons in Fed Mice Enables Conditioned Food Seeking under
861 Threat. *Current Biology*, *26*(18), 2500–2507. https://doi.org/10.1016/J.CUB.2016.07.019

862 Kim, S. Y., Adhikari, A., Lee, S. Y., Marshel, J. H., Kim, C. K., Mallory, C. S., Lo, M., Pak, S.,
863 Mattis, J., Lim, B. K., Malenka, R. C., Warden, M. R., Neve, R., Tye, K. M., & Deisseroth,
864 K. (2013). Diverging neural pathways assemble a behavioural state from separable
865 features in anxiety. *Nature 2013 496:7444*, *496*(7444), 219–223.
866 https://doi.org/10.1038/nature12018

867 Krashes, M. J., Koda, S., Ye, C. P., Rogan, S. C., Adams, A. C., Cusher, D. S., Maratos-Flier,
868 E., Roth, B. L., & Lowell, B. B. (2011). Rapid, reversible activation of AgRP neurons
869 drives feeding behavior in mice. *Journal of Clinical Investigation*, *121*(4), 1424–1428.
870 https://doi.org/10.1172/JCI46229

871 Krashes, M. J., Shah, B. P., Madara, J. C., Olson, D. P., Strochlic, D. E., Garfield, A. S.,
872 Vong, L., Pei, H., Watabe-Uchida, M., Uchida, N., Liberles, S. D., & Lowell, B. B. (2014).
873 An excitatory paraventricular nucleus to AgRP neuron circuit that drives hunger. *Nature*
874 *2014 507:7491*, *507*(7491), 238–242. https://doi.org/10.1038/nature12956

875 Krnjević, K., & Schwartz, S. (1967). The action of γ-Aminobutyric acid on cortical neurones.
876 *Experimental Brain Research*, *3*(4), 320–336. https://doi.org/10.1007/BF00237558

Li, C., Hou, Y., Zhang, J., Sui, G., Du, X., Licinio, J., Wong, M. L., & Yang, Y. (2019). AGRP neurons modulate fasting-induced anxiolytic effects. *Translational Psychiatry 2019 9:1*, *9*(1), 1–10. https://doi.org/10.1038/s41398-019-0438-1

Lin, J. Y., Lin, M. Z., Steinbach, P., & Tsien, R. Y. (2009). Characterization of Engineered Channelrhodopsin Variants with Improved Properties and Kinetics. *Biophysical Journal*, *96*(5), 1803–1814. https://doi.org/10.1016/J.BPJ.2008.11.034

Lindroos, R., & Hellgren Kotaleski, J. (2021). Predicting complex spikes in striatal projection neurons of the direct pathway following neuromodulation by acetylcholine and dopamine. *The European Journal of Neuroscience*, *53*(7), 2117–2134. https://doi.org/10.1111/ejn.14891

Liu, J., Conde, K., Zhang, P., Lilascharoen, V., Xu, Z., Lim, B. K., Seeley, R. J., Zhu, J. J., Scott, M. M., & Pang, Z. P. (2017). Enhanced AMPA receptor trafficking mediates the anorexigenic effect of endogenous glucagon like peptide-1 in the paraventricular hypothalamus. *Neuron*, *96*(4), 897. https://doi.org/10.1016/J.NEURON.2017.09.042

Ludwig, M. Q., Cheng, W., Gordian, D., Lee, J., Paulsen, S. J., Hansen, S. N., Egerod, K. L., Barkholt, P., Rhodes, C. J., Secher, A., Knudsen, L. B., Pyke, C., Myers, M. G., & Pers, T. H. (2021). A genetic map of the mouse dorsal vagal complex and its role in obesity. *Nature Metabolism*, *3*(4), 530–545. https://doi.org/10.1038/s42255-021-00363-1

Luquet, S., Perez, F. A., Hnasko, T. S., & Palmiter, R. D. (2005). NPY/AgRP neurons are essentials for feeding in adult mice but can be ablated in neonates. *Science*, *310*(5748), 683–685. https://doi.org/10.1126/SCIENCE.1115524

Luquet, S., Phillips, C. T., & Palmiter, R. D. (2007). NPY/AgRP neurons are not essential for feeding responses to glucoprivation. *Peptides*, *28*(2), 214–225. https://doi.org/10.1016/J.PEPTIDES.2006.08.036

Madisen, L., Zwingman, T. A., Sunkin, S. M., Oh, S. W., Zariwala, H. A., Gu, H., Ng, L. L., Palmiter, R. D., Hawrylycz, M. J., Jones, A. R., Lein, E. S., & Zeng, H. (2009). A robust and high-throughput Cre reporting and characterization system for the whole mouse brain. *Nature Neuroscience 2009 13:1*, *13*(1), 133–140. https://doi.org/10.1038/nn.2467

Mandelblat-Cerf, Y., Ramesh, R. N., Burgess, C. R., Patella, P., Yang, Z., Lowell, B. B., & Andermann, M. L. (2015). Arcuate hypothalamic AgRP and putative POMC neurons

907 show opposite changes in spiking across multiple timescales. *ELife*, *4*.
908 https://doi.org/10.7554/eLife.07122

909 Olson, B. R., Freilino, M., Hoffman, G. E., Stricker, E. M., Sved, A. F., & Verbalis, J. G. (1993).
910 C-Fos expression in rat brain and brainstem nuclei in response to treatments that alter
911 food intake and gastric motility. *Molecular and Cellular Neurosciences*, *4*(1), 93–106.
912 https://doi.org/10.1006/MCNE.1993.1011

913 Petreanu, L., Huber, D., Sobczyk, A., & Svoboda, K. (2007). *Channelrhodopsin-2-assisted*
914 *circuit mapping of long-range callosal projections*. https://doi.org/10.1038/nn1891

915 Richard, C. D., Tolle, V., & Low, M. J. (2011). Meal pattern analysis in neural-specific
916 proopiomelanocortin-deficient mice. *European Journal of Pharmacology*, *660*(1), 131–
917 138. https://doi.org/10.1016/J.EJPHAR.2010.12.022

918 Shi, M. Y., Ding, L. F., Guo, Y. H., Cheng, Y. X., Bi, G. Q., & Lau, P. M. (2021). Long-range
919 GABAergic projections from the nucleus of the solitary tract. *Molecular Brain*, *14*(1), 1–
920 5. https://doi.org/10.1186/S13041-021-00751-4/FIGURES/1

921 Spruston, N., Jaffe, D. B., Williams, S. H., & Johnston, D. (1993). Voltage- and space-clamp
922 errors associated with the measurement of electrotonically remote synaptic events.
923 *Journal of Neurophysiology*, *70*(2), 781–802. https://doi.org/10.1152/jn.1993.70.2.781

924 Stamatakis, A. M., & Stuber, G. D. (2012). Activation of lateral habenula inputs to the ventral
925 midbrain promotes behavioral avoidance. *Nature Neuroscience 2012 15:8*, *15*(8), 1105–
926 1107. https://doi.org/10.1038/nn.3145

927 Sylantyev, S., Savtchenko, L. P., O'Neill, N., & Rusakov, D. A. (2020). Extracellular GABA
928 waves regulate coincidence detection in excitatory circuits. *The Journal of Physiology*,
929 *598*(18), 4047. https://doi.org/10.1113/JP279744

930 Tsang, A. H., Nuzzaci, D., Darwish, T., Samudrala, H., & Blouet, C. (2020). Nutrient sensing
931 in the nucleus of the solitary tract mediates non-aversive suppression of feeding via
932 inhibition of AgRP neurons. *Molecular Metabolism*, *42*, 101070.
933 https://doi.org/10.1016/J.MOLMET.2020.101070

934 van den Pol, A. N., Yao, Y., Fu, L. Y., Foo, K., Huang, H., Coppari, R., Lowell, B. B., &
935 Broberger, C. (2009). Neuromedin B and gastrin-releasing peptide excite arcuate
936 nucleus neuropeptide Y neurons in a novel transgenic mouse expressing strong Renilla

937 green fluorescent protein in NPY neurons. *The Journal of Neuroscience : The Official*
938 *Journal of the Society for Neuroscience*, *29*(14), 4622–4639.
939 https://doi.org/10.1523/JNEUROSCI.3249-08.2009

940 Vong, L., Ye, C., Yang, Z., Choi, B., Chua, S., & Lowell, B. B. (2011). Leptin action on
941 GABAergic neurons prevents obesity and reduces inhibitory tone to POMC neurons.
942 *Neuron*, *71*(1), 142–154. https://doi.org/10.1016/J.NEURON.2011.05.028

943 Wagner, S., Brierley, D. I., Leeson-Payne, A., Jiang, W., Chianese, R., Lam, B. Y. H.,
944 Dowsett, G. K. C., Cristiano, C., Lyons, D., Reimann, F., Gribble, F. M., Martinez de
945 Morentin, P. B., Yeo, G. S. H., Trapp, S., & Heisler, L. K. (2022). Obesity medication
946 lorcaserin activates brainstem GLP-1 neurons to reduce food intake and augments GLP-
947 1 receptor agonist induced appetite suppression. *Molecular Metabolism*, *68*.
948 https://doi.org/10.1016/J.MOLMET.2022.101665

949 Wang, C., Zhou, W., He, Y., Yang, T., Xu, P., Yang, Y., Cai, X., Wang, J., Liu, H., Yu, M.,
950 Liang, C., Yang, T., Liu, H., Fukuda, M., Tong, Q., Wu, Q., Sun, Z., He, Y., & Xu, Y.
951 (2021). AgRP neurons trigger long-term potentiation and facilitate food seeking.
952 *Translational Psychiatry*, *11*, 11. https://doi.org/10.1038/s41398-020-01161-1

953 Williams, D. L., & Schwartz, M. W. (2005). The melanocortin system as a central integrator
954 of direct and indirect controls of food intake. *American Journal of Physiology. Regulatory,*
955 *Integrative and Comparative Physiology*, *289*(1).
956 https://doi.org/10.1152/AJPREGU.00226.2005

957 Wu, Q., Lemus, M. B., Stark, R., Bayliss, J. A., Reichenbach, A., Lockie, S. H., & Andrews,
958 Z. B. (2014). The Temporal Pattern of cfos Activation in Hypothalamic, Cortical, and
959 Brainstem Nuclei in Response to Fasting and Refeeding in Male Mice. *Endocrinology*,
960 *155*(3), 840–853. https://doi.org/10.1210/EN.2013-1831

961 Yavari, A., Stocker, C. J., Ghaffari, S., Wargent, E. T., Steeples, V., Czibik, G., Pinter, K.,
962 Bellahcene, M., Woods, A., Martinez de Morentin, P. B., Cansell, C., Lam, B. Y., Chuster,
963 A., Petkevicius, K., Nguyen-Tu, M. S., Martinez-Sanchez, A., Pullen, T. J., Oliver, P. L.,
964 Stockenhuber, A., … Ashrafian, H. (2016). Chronic Activation of gamma2 AMPK Induces
965 Obesity and Reduces beta Cell Function. *Cell Metab*, *23*(5), 821–836.
966 https://doi.org/10.1016/j.cmet.2016.04.003

967 Zhan, C., Zhou, J., Feng, Q., Zhang, J. en, Lin, S., Bao, J., Wu, P., & Luo, M. (2013). Acute
968 and long-term suppression of feeding behavior by POMC neurons in the brainstem and
969 hypothalamus, respectively. *The Journal of Neuroscience : The Official Journal of the*
970 *Society for Neuroscience*, *33*(8), 3624–3632.
971 https://doi.org/10.1523/JNEUROSCI.2742-12.2013

972 Zingg, B., Chou, X. lin, Zhang, Z. gang, Mesik, L., Liang, F., Tao, H. W., & Zhang, L. I. (2017).
973 AAV-Mediated Anterograde Transsynaptic Tagging: Mapping Corticocollicular Input-
974 Defined Neural Pathways for Defense Behaviors. *Neuron*, *93*(1), 33–47.
975 https://doi.org/10.1016/J.NEURON.2016.11.045

976 Zorrilla, E. P., Inoue, K., Fekete, É. M., Tabarin, A., Valdez, G. R., & Koob, G. F. (2005).
977 Measuring meals: Structure of prandial food and water intake of rats. *American Journal*
978 *of Physiology - Regulatory Integrative and Comparative Physiology*, *288*(6 57-6), 1450–
979 1467.
980 https://doi.org/10.1152/AJPREGU.00175.2004/SUPPL_FILE/ZORRILLA_SUPP_TABL
981 E.PDF

982